Chapter 22
Energy Storage for Medium- to Large-Scale Applications

22.1 Introduction

Most of the highly visible applications of advanced energy storage technologies are for relatively small applications, such as in portable computers or implanted medical devices, where the paramount issue is the amount of energy stored per unit weight or volume, and cost is not always of prime importance. Such energy storage components and systems have occupied much of the attention in this text, especially the later chapters related to electrochemical cells and systems.

As discussed in Chap. 1, there are several types of large-scale energy storage applications that have unique characteristics, and thus require storage technologies that are significantly different from the smaller systems that are most common at the present time. These include utility load leveling, solar and wind energy storage, and vehicle propulsion. They play critical roles in the transition away from the dependence upon fossil fuels.

More than for smaller scale applications, the important factors in large systems are the cost per unit energy storage, e.g., per kWh, efficiency of the energy storage cycle, which has a large influence upon operating costs, and the lifetime of the critical components. Investors generally expect large systems to be in operation for 25 years or more. In addition, great attention is paid to safety matters.

Several of the storage technologies that are particularly interesting and important for larger-scale applications are described in the early chapters of this book. Some others are discussed in this chapter.

R.A. Huggins, *Energy Storage*, DOI 10.1007/978-3-319-21239-5_22

22.2 Utility Load Leveling, Peak Shaving, and Transients

The requirements of the large-scale electrical distribution network, or grid, are discussed in Chap. 1. The major problem is to match the energy available to the needs, which typically undergo daily, weekly, and seasonal variations. In addition, there are short-term transients that can lead to instabilities and other problems with the electrical power grid. The amelioration of these problems requires not only better technology, but also an intelligent control system to couple energy generation, transmission, and storage. Major factors include cost, reliability, lifetime, efficiency, and safety.

The energy storage method that is most widely used to reduce the longer-term variations in some areas involves the use of pumped-hydro facilities discussed in Chap. 6. However, this is only possible in specific locations, where the required geological features are present. Large-scale underground compressed air storage systems also have important location requirements. Although they are often discussed, very few are in actual operation at the present time.

Other technologies can be useful in reducing the impact of short-term transients, which are now handled primarily by variation of the AC output frequency. One of these, also discussed in Chap. 6, involves the use of very large flywheels. Some of these are now available with power values up to 100 kW. The integration of a number of such units to provide total power up to 20 MW is being investigated. The Department of Energy has estimated that 100 MW of flywheel storage could eliminate 90 % of the frequency variations in the State of California.

Additional approaches that are being explored at present involve reversible high power electrochemical systems. Here, the amount of energy stored per unit cost is of prime importance. In contrast to other uses of electrochemical systems, the size and weight are generally not important for this type of application. Several of these are discussed later in this chapter.

22.3 Storage of Solar- and Wind-Generated Energy

Solar and wind energy sources are often viewed as technologies that can be both employed to satisfy transient local needs, and to supply energy into the electricity distribution grid. However, their output generally only roughly matches the time-dependent requirements of the grid. Thus energy storage mechanisms are required to assist their integration into that large-scale system. Short-term transients in their output, such as when a cloud passes over a solar collection system, or the wind drops in velocity, are generally not of great importance for that application.

For applications such as matching the time dependence of the needs and supplies of energy in the large-scale electricity grid, some relatively low cost electrochemical systems, that are not interesting for portable applications because of their size or weight, can be advantageous.

22.4 Several Recent Developments That May Be Useful for These Applications

22.4.1 Hybrid Lead-Acid Batteries for Large Scale Storage

Pb-acid batteries, due to their relative ease of manufacture, and favorable electrochemical characteristics, such as rapid kinetics and relatively good cycle life, are commonly used for automotive starting. The low cost per unit energy stored is a particularly attractive feature of this type of technology. Large groups of them are being used to support solar and wind generation systems.

As described in Chap. 17, conventional Pb-acid cells are typically kept at or near a full state of charge, but they tend to deteriorate quickly when operated at a partial state of charge. This limits their utility in a number of other applications.

This situation has changed recently, due to the development of lead-acid cells with a double negative electrode design that leads to a device that has properties that are a combination of a standard lead-acid battery and an ultracapacitor. The result of this approach is that these cells can operate for long periods of time at a partial state of charge. The label "UltraBattery" is being used by the suppliers of this technology.

The UltraBattery was invented in 2003 by Dr. Lan Lamm and his team at the Commonwealth Scientific and Industrial Research Organization (CSIRO) in Australia, where some initial production began in 2005. The firm Ecoult was formed by CSIRO in 2007 to commercialize this technology.

In 2010 Ecoult was purchased from CSIRO by East Penn Manufacturing, Inc. in the United States. The Japanese firm Furukawa Battery acquired a license for this technology in Japan and Thailand from CSIRO, but East Penn has a license for the rest of the world.

The UltraBattery is a hybrid energy storage device that combines a single positive electrode, comparable to that used in normal Pb-acid cells, with a double negative electrode—one part containing lead, and the other part carbon, in a common sulfuric acid electrolyte. This is illustrated schematically in Fig. 22.1.

This is important in applications such as their use in hybrid vehicles, where both braking (high rate charging) and acceleration (high rate discharging) can occur in rapid repetition for many thousands of cycles.

It is predicted that it is reasonable to expect that these batteries will last more than 40,000 cycles, some 10 times longer than the shallow cycles of conventional Pb-acid batteries, and more than 4 times longer than a Pb-acid battery designed specifically for idling-stop-start vehicles.

This hybrid technology provides more power and a longer lifespan than standard Pb-acid batteries and it is claimed that this technology can provide performance similar to that of metal hydride/nickel batteries, but at a significantly lower cost.

This modified version of the Pb-acid system also suffers significantly less from the development of permanent (or hard) $PbSO_4$ deposits (typically called

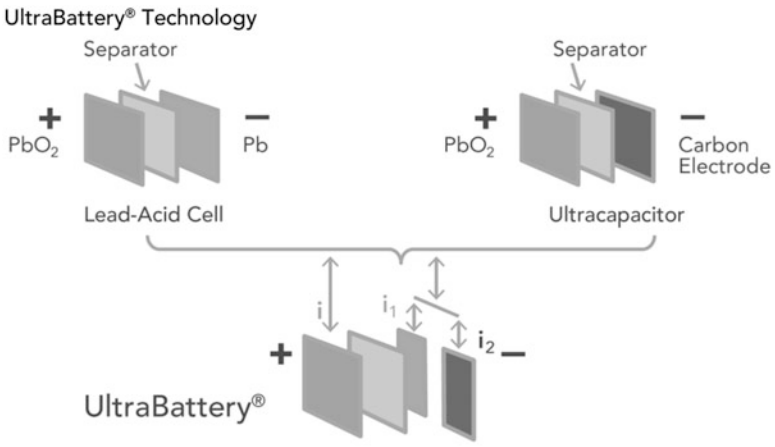

Fig. 22.1 General layout of an UltraBattery

"sulfation") on the negative battery electrode—a problem commonly exhibited in conventional lead acid batteries when they are used for stand-by applications.

The standard solution to this problem is the use of occasional "refresh cycles," in which they are charged, typically at a 1C rate, followed by a lengthy period of lower-rate charging at a "float" voltage so that all cells reach 100 % state of charge. This helps restore the physical state of the electrodes and allows individual battery cells to attain consistent voltages and state of charge, when otherwise they might diverge during an extended period of cycling. A refresh cycle concludes when the battery is returned to the state of charge required by the application it is serving.

During a refresh cycle, therefore, the battery is not in operation, so it is desirable to minimize this downtime. It has been shown that an UltraBattery can operate for more than ten times as many cycles between recovery charges than standard Pb-acid batteries.

Tests on hybrid electric vehicles (HEVs) showed a range of more than 100,000 miles on a single battery pack without significant degradation.

A major disadvantage of conventional Pb-acid batteries is that they are typically designed for uses in which they are kept close to fully charged. Long periods in a partial state of charge cause severe decay in their capacity.

Because they can operate at a partial state of charge, UltraBatteries are also ideally suited to provide frequency regulation services to the grid. They can respond in both directions by charging or discharging rapidly and can ramp much faster than any conventional generator, following the regulation control signal accurately.

This type of battery can be used in advanced hybrid vehicles that have an "idling-stop" function that stops the internal combustion engine when the vehicle stops. Such vehicles also typically use regenerative braking to recover some of the vehicle's energy of motion to help charge the battery. With these innovations the fuel efficiency is typically increased by approximately 10 % compared to a non-hybrid vehicle

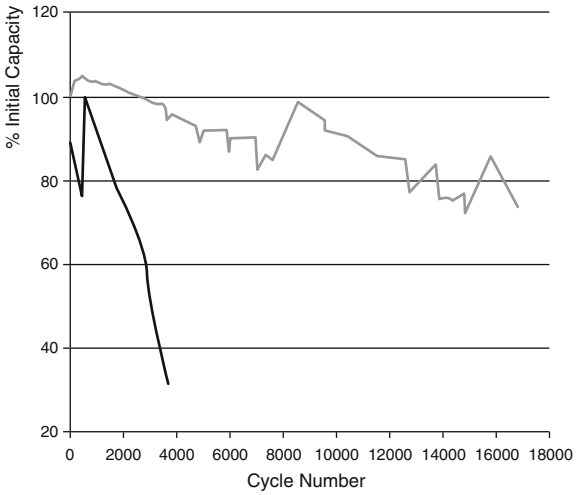

Fig. 22.2 Longevity under high-rate partial state of charge cycling tests [1]

To accept charge from regenerative braking efficiently, the battery is kept at a partial state of charge, typically about 90 % of its full capacity, and it must be able to withstand both high discharging and charging rates. This contrasts with non-hybrid vehicles, in which the battery floats on full charge, using the alternator to provide mild charging rates. If the engine must be restarted when the driver releases the brake pedal after stopping, the number of large-current discharges can be many more than is typical in non-hybrid vehicles.

Some hybrid vehicles also use their batteries to provide electric propulsion to assist the internal combustion engine during operation in addition to idling-stop and regenerative braking. This can increase the fuel efficiency by approximately 20–25 % compared to a non-hybrid vehicle.

A further area of application of this enhanced Pb-acid battery technology involves the support of solar and wind systems to relieve the inherent variability in their energy generation.

Reserve battery capacity can be used to alleviate output shortfalls for short time scales: minutes or even seconds. This reduces the need to have large "spinning reserve" generators, which are typically used for this purpose (Fig. 22.2).

Field driving tests have demonstrated that there is no difference between the driving performance of a hybrid vehicle using an UltraBattery pack and one using a metal hydride/nickel battery pack. But the cost of an UltraBattery pack is dramatically less than the metal hydride/nickel pack.

To follow up and further quantify the road test results, laboratory cycle-life tests were conducted on 2 V cell flooded type UltraBatteries based on the power-assisting EUCAR profile [2, 3]. The tests were started at a 60 % state of charge, and no recovering charging was performed. The life of the UltraBatteries was more than 40,000 cycles, representing a cycle life more than ten times that of a

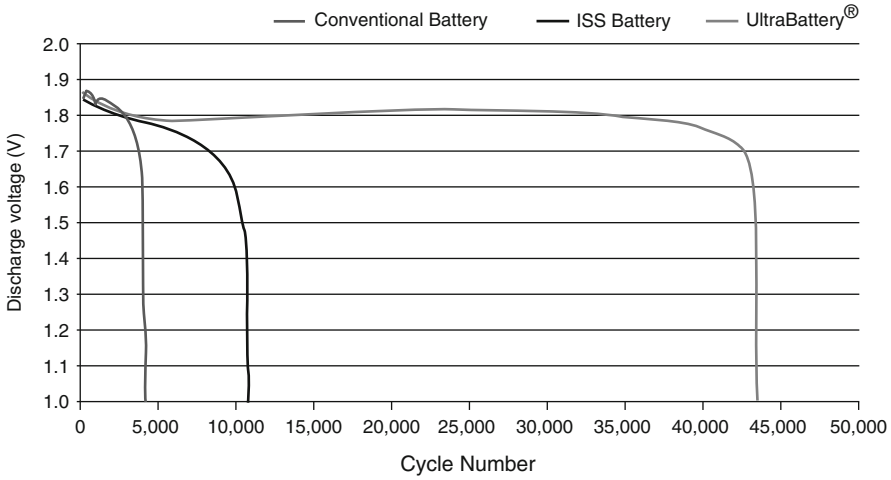

Fig. 22.3 Cycling performance of a conventional Pb-acid battery, an ISS battery, and an UltraBattery when used under a standard driving profile [3]

conventional lead-acid battery, and more than four times longer than that of a lead-acid battery specifically designed for idling-stop-start (ISS) vehicles. This is shown in Fig. 22.3.

22.5 Batteries with Open Framework Crystal Structure Electrodes

22.5.1 Introduction

As mentioned in Chap. 13, it has been known for some 25 years that charge can be stored in some important battery electrodes by the insertion of ionic species from the electrolyte. Insertion reactions play an especially important role in current versions of lithium batteries, where lithium cations are typically the inserted species in both electrodes. This is also true of a number of other lithium-containing materials. Hydrogen cations (protons) are the inserted guest species during the operation of other types of battery electrodes, including the $Ni(OH)_2/NiOOH$ electrode, the "MnO_2" electrode, and RuO_2 in aqueous systems.

Whereas most attention has been given to materials in which the guest species are cations, it is also possible to have anion insertion into some crystal structures. Materials in which the structure can accommodate *either* cations or anions are especially interesting.

There also are some cases in which *both* cations and anions can be inserted into a crystal structure. One example of this type is briefly discussed in this chapter, ternary materials with the hexagonal transition metal bronze structure.

Most attention is given here to the hexacyanometallate family of materials, however. These materials have structures which are variants of the cubic ReO_3 type of crystal structure which have rather large inter-cell windows. They can accommodate a wide variety of guest ions of both charges. Cations can be inserted into the structure at relatively low potentials, and anions can be inserted at more positive potentials. This can lead to a number of interesting features and properties.

22.5.2 Insertion of Guest Species Into Materials with Transition Metal Oxide Bronze Structures

It has long been known that a number of ions can be readily inserted into the structures of ternary oxides such as the tungsten, molybdenum and vanadium bronzes. These bronze families can exist in several different crystal structures, depending upon the identity and concentration of the lower-charge cations present. If the inserted ions are relatively small, these materials often have the cubic ReO_3 structure.

Especially interesting, however, are materials with the hexagonal tungsten bronze structure with the general formula M_xWO_3, in which there are two types of crystallographic tunnels. There is a hexagonal array of rather large linear tunnels that penetrate through the structure parallel to the c-axis. This structure is only obtained when M is a large cation, such as K^+, Rb^+, or Cs^+. K_xWO_3, where $x = 0.3$ and the K^+ ions partly occupy the positions in the large tunnels. They can be readily prepared by either solid state or electrochemical methods at elevated temperatures. This structure is shown schematically in Fig. 22.4.

This material is dark blue-black, due to the presence of both W^{5+} and W^{6+} species. If it is heated to intermediate temperatures (e.g., 400 °C) in air O^{2-} anions are introduced into the large tunnels. These balance the charge of the K^+ ions, causing all the tungsten ions to become W^{6+}. The material is thus bleached, becoming white.

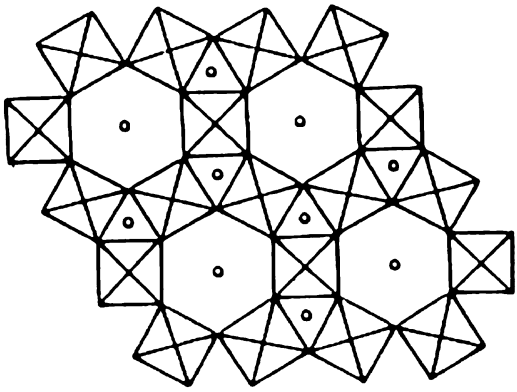

Fig. 22.4 Representation of the hexagonal tungsten bronze structure in the c-direction, small circles show the presence of both large and small tunnel sites

Li^+ cations can subsequently be inserted into this structure at room temperature. They go into the set of smaller tunnels that are oriented in the cross-direction, rather than into the large tunnels. The presence of the lithium ions causes the reduction of some of W^{6+} ions to W^{5+}, and the material becomes dark. Thus the low temperature insertion of Li^+ cations, which is both very rapid and reversible, can be employed to make this an interesting electrochromic material [4–7]. However, because of its cost and weight, it is not a practical alternative for use in batteries.

22.5.3 *Materials with Cubic Structures Related to Rhenium Trioxide*

Another crystal structure that can have interesting properties of this type is the ReO_3 (or BX_3) structure, which has cubic symmetry. This structure can be thought of as a simple cubic arrangement of corner-shared octahedral BX_6 groups. There is empty space in the center of each of these cubes that is interconnected by a three-dimensional set of tunnels through the centers of the cube faces. It is possible for this cube-center space to be either empty, partly, or fully occupied by cations, assuming that the charges of the other species present are adjusted so as to maintain overall charge neutrality

If there is a cation in the center of every cube, the nominal formula is then ABX_3, and this is the well-known perovskite structure, which is adopted by many oxides. In order for it to be stable, the A ions must be relatively large. The more highly charged B ions are quite small.

It has been shown that a variety of ions can reside on the A sites of this structure. In addition, there may be mixed occupation by more than one type of ion. An example of this is the family of Li-La titanates, in which lithium ions, lanthanum ions, and vacancies are distributed among the available A sites. It has been shown that these materials can have a relatively high lithium ionic conductivity at positive potentials [8–12], and that they are also interesting fast mixed-conductors at more negative potentials [13].

22.5.4 *Aqueous Batteries with Manganese Oxide Electrodes with Crystallographic Channels*

A different type of rechargeable aqueous battery system has received considerable attention in recent years. It is based upon the use of a sodium manganese oxide in the positive electrode that has a crystal structure in which sodium ions can enter and leave from the electrolyte rapidly.

Recognition of the potential for the use of this material in a new type of practical and inexpensive rechargeable battery by Prof. J. Whitacre at Carnegie Mellon

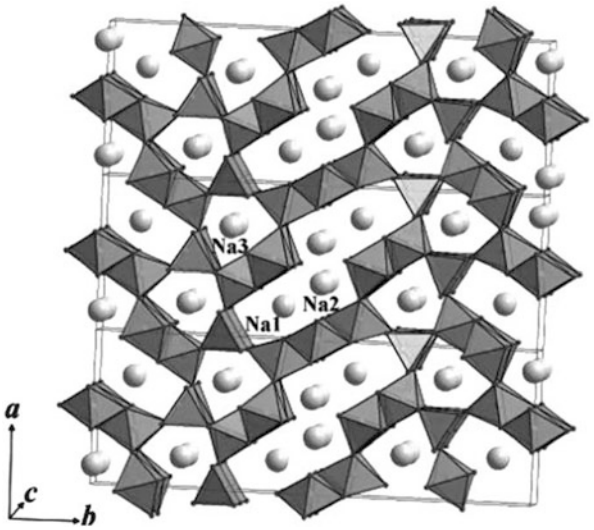

Fig. 22.5 Model of the crystal structure showing the locations of the sodium ions in the channels between the manganese-centered octahedra and square pyramidal units in the structure [14]

University led to the formation of the firm Aquion in 2010 to commercialize this technology.

The key element is the use of the phase whose composition can be written either as $Na_4Mn_9O_{18}$, or more simply, as $Na_{0.44}MnO_2$, as the positive electrode reactant. This material has an orthorhombic crystal structure that can be described as containing both MnO_6 octahedra and MnO_5 square pyramids. These form a special arrangement that contains interconnected channels with two different types of atomic-sized locations for the sodium ions. In one case, the sodium ions sit in sites that are interconnected. As a result, they are mobile, and can be reversibly extracted from the crystal structure and reinserted. Those in the other type of location in the structure are not mobile.

The characteristics of this structure can be seen in Fig 22.5. Examples of mobile ion positions are indicated as Na1 and Na2. Ions in Na3 type positions cannot readily move through the crystal structure [14].

There was some earlier interest in the behavior of this material as an electrode reactant in lithium ion systems [15, 16], but its properties as an electrode in sodium systems are much more attractive [17–21].

This material has an inherently low cost. Fine particle electrodes with a high surface area can be produced from it inexpensively using processes that are readily scalable. They can be made into rather thick porous electrode structures through which the high conductivity aqueous electrolyte can readily transport the transport of sodium ions.

An aqueous solution of sodium sulfate, which has a very high ionic conductivity, is used as the electrolyte. Since this electrolyte has negligible electronic leakage,

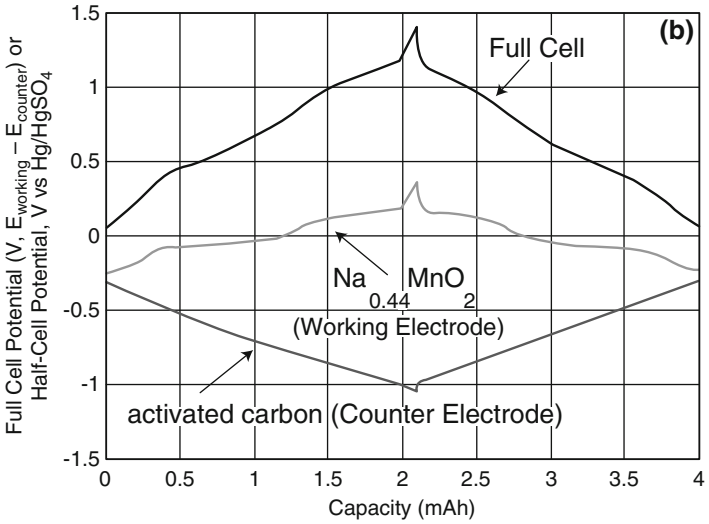

Fig 22.6 Variation of the cell voltage and individual electrode potentials with the state of charge [17]

self-discharge is quite low. Electronic short circuits between the electrodes are prevented by the presence of an inexpensive porous nonwoven cellulose separator.

The negative electrode in the Aquion batteries is produced from inexpensive finely divided activated carbon. This material stores ions reversibly deposited from the electrolyte onto its surface, and has the characteristics of a simple capacitor, with an electric potential that is essentially a linear function of the charge.

The variation of the electrode potentials, as well as the full cell voltage, with the state of charge in this system is shown in Fig. 22.6. It can be seen that there are two semi-plateau regions in the potential of the positive electrode in different potential regimes. This indicates the presence of two reactions, centered at different potentials. This conclusion is consistent with the results of cyclic voltammetric experiments shown in Fig. 22.7, which clearly shows reactions in two distinct potential regions.

Cell discharge curves at different rates are shown in Fig. 22.8. It is seen that the total capacity—down to a minimum value of 0.3 V—varies significantly with the discharge rate, as does the output voltage.

The manufacturing processes involved in this technology are inexpensive and readily scalable, and projected costs are low, less than $ 300 per kWh. Aquion is constructing a manufacturing plant to produce 500 megawatt-hours of these batteries per year near Pittsburgh, PA

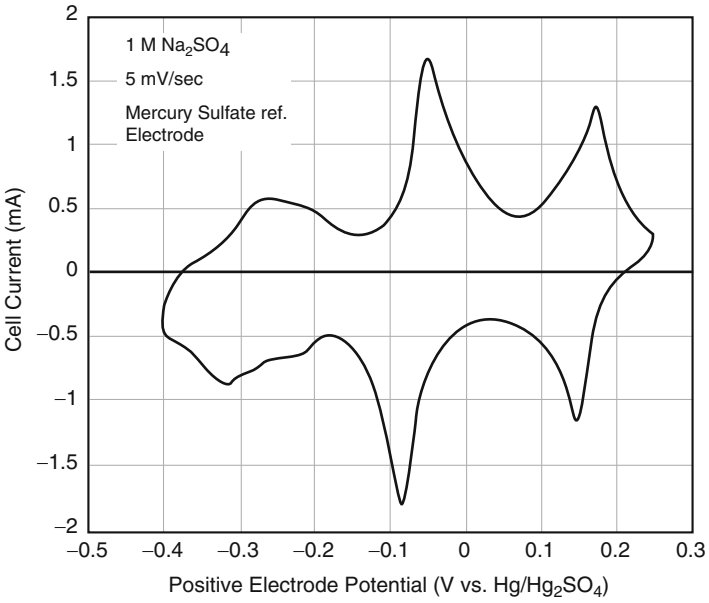

Fig. 22.7 Cyclic voltammetry measurements on $Na_{0.44}MnO_2$ [17]

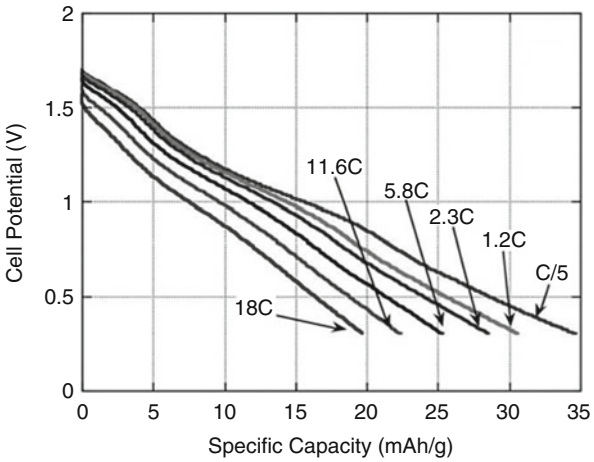

Fig 22.8 Cell potential as a function of the state of charge from experiments at different rates of discharge [17]

Their initial commercial target is to produce multi-cell systems for small niche markets, such as off-grid solar and wind installations. A cycle life over 5000 cycles at 60 % depth of discharge, with an energy efficiency over 85 % has been demonstrated, which should be satisfactory for this purpose.

22.6 Hexacyanometallate Electrode Materials

22.6.1 Introduction

There is a family of materials with crystal structures that are analogous to the BX_3 rhenium trioxide and ABX_3 perovskite materials, but in which the X positions are occupied by cyanide anions, which are appreciably larger than oxide ions. These materials are sometimes called hexacyanometallates, and the B positions are often occupied by transition metal ions. The transition metal hexacyanometallates are examples of the large family of insoluble mixed-valence compounds with interesting properties [22, 23]. An earlier, and more extensive, overview of some aspects of these materials can be found in the paper by Robin and Day [24].

The prototype material is "Prussian blue," which is also sometimes called "Berlin blue." Its nominal formula is $KFe_2(CN)_6$, or $K_{0.5}Fe(CN)_3$. It has a dark blue-black color, has been known for a very long time, and has been widely used as a dyestuff. It was evidently the first coordination compound reported in the scientific literature [25]. An account of the early work on the preparation and chemical composition of materials in the Prussian blue family can be found in ref. [26]. They have been studied extensively because of their electrochromic properties, and there has been renewed interest in them in recent years in connection with their use in "modified electrode surfaces" that are interesting for catalytic purposes.

22.6.2 The Structure of The Prussian Blues

The general formula for materials in this family is $A_xP^{3+}R^{2+}(CN)_6$, where the P^{3+} and R^{2+} species are distributed in an ordered arrangement upon the B sites of the A_xBX_3 structure. The value of x, which specifies the amount of A present, can often be varied from 0 to 2. When $x = 0$ the material has the ReO_3 (BX_3) structure, and when $x = 2$, the structure is analogous to the ABX_3 perovskites. In the case of Prussian blue, the A sites are half full, and x is nominally equal to 1.

The structure of Prussian blue was first discussed by Keggin and Miles in 1936 [27], on the basis of powder x-ray diffraction results. They found it to be cubic, like the ReO_3 and perovskite materials, with a simple cube edge length about 5.1 A. In normal Prussian blue K^+ ions fill half of the A positions, and Fe ions are in the B positions. In order to keep overall charge balance, half of the Fe ions have a formal charge of 3+ (and thus can be described as P^{3+} ions), and half have a formal charge of 2+ (and can be described as R^{2+} ions). The carbon ends of the CN^- ions point toward the Fe^{2+} ions, and the nitrogen ends toward the Fe^{3+} ions. Thus one can think of the P^{3+} ions being in a nitrogen-surrounded hole, and the R^{2+} being in a carbon-surrounded hole, in the structure. This structure is shown schematically in Figs. 22.9 and 22.10.

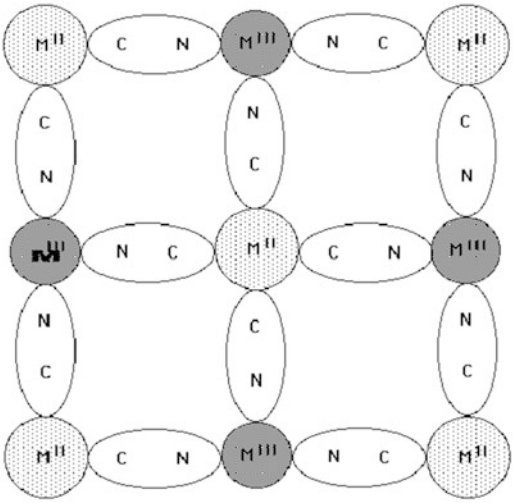

Fig. 22.9 Schematic representation of one plane in the structure of the hexacyanometallate host lattice

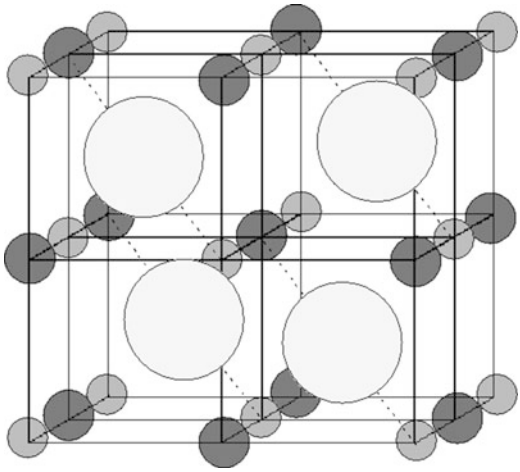

Fig. 22.10 Schematic representation of the structure of Prussian blue, in which half of the A sites are filled

It can readily be seen that these two general formulas lead to different structural interpretations. If the composition of the "insoluble" alternative, $Fe_4[Fe(CN)_6]_3$, is correct, it can be written as $Fe^{3+}{}_4Fe^{2+}{}_3(CN)_{18}$ or $(Fe^{3+})_{1/3}(Fe^{3+}Fe^{2+})\ (CN)_6$. This would indicate that 1/6 of the A positions are occupied by Fe^{3+} ions, instead of their being half-filled with K^+ ions in the "soluble" version. The presence of hydrated Fe^{3+} ions at the A sites has been reported by [28].

Although incorporated water is not included in the compositional formulas of materials in this family, are of them are generally found to contain substantial amounts of water when they are prepared by the use of aqueous methods. When some ethanol is present in the water, the behavior changes somewhat, indicating an influence of the co-absorbed species [29]. It has also been found that the behavior is very different in nonaqueous electrolytes, such as propylene carbonate [30]. The presence of even a relatively small amount of water (e.g., 1 vol %) in such nonaqueous electrolytes leads to behavior quite similar to that found in aqueous electrolytes. This provides strong evidence for the importance of the hydration sheath around the insertable cations in the A position in the structure.

On the other hand, water-free materials can also be produced using solid state methods [31]. The dry-produced materials with high values of x are very sensitive to moisture and oxidation in air, turning blue and undergoing decrepitation.

Because of the possibility that the ions on the two types of B sites may have variable valences these materials can often be either reduced or oxidized, or both. The mechanism whereby this occurs involves the insertion or removal of charged species on the A sites.

Reduction can occur by increasing the concentration of A^+ ions in the structure. In the case that both P and R species are Fe ions, the additional positive charge in the A sites is balanced by the reduction of some of the Fe^{3+} species on the P sites to Fe^{2+}. When the A^+ concentration reaches 2, essentially all of the Fe^{3+} ions have been reduced, so that there are Fe^{2+} ions on both the P and R sites. Thus the composition can be written as $A_2P^{2+}R^{2+}(CN)_6$.

Prussian blue and its analogs can also be oxidized by the removal of A^+ species. In this case the decreased positive charge on the A sites is balanced by the oxidation of Fe^{2+} species on the R positions to Fe^{3+}, and the nominal composition becomes $P^{3+}R^{3+}(CN)_6$. Thus we see that Fe ions can participate in both reduction and oxidation processes as the concentration of positively charged A^+ ions is varied.

In addition to the (complete) removal of the A^+ species, the structure can be further oxidized by the insertion of negatively charged anionic species (B^-) into the A sites. In this case the composition can be nominally described as $A_xP^{3+}R^{3+}(CN)_6B_y$, where x is 0.

Thus these materials can have insertion of either cations or anions into the A sites, depending upon the potential. The insertion kinetics depend greatly upon the identity of the inserted species. In some cases this can be remarkably rapid. Due to the large size of the CN^- anions, the openings between adjacent unit cells are quite large. Thus it is possible for relatively large ions to move throughout the structure by jumping through these windows. Species in the A sites are often highly mobile, and can be accompanied by an appreciable amount of water of hydration.

These hexacyanoferrates are generally stable in water at low to moderate values of pH. In acidic electrolytes containing K^+ ions they can be reduced and reoxidized many times, and show excellent reversibility. Over 10^7 cycles have been demonstrated in some cases [32–34].

22.6.3 Electrochemical Behavior of Prussian Blue

Prussian blue and its analogs can be readily reduced and oxidized electrochemically. Much of the experimental work in the literature on the electrochemical behavior of Prussian blue has been performed using potassium-containing aqueous electrolytes with a pH value of about 4, and potentials are generally referenced to the standard calomel electrode (SCE), which is about 478 mV positive of the reversible hydrogen evolution electrode potential at that value of pH. Although very common, this choice of reference electrode is unfortunate, as the definition of its potential relative to neutral chemical species requires knowledge of the pH, in accordance with the Gibbs Phase Rule, as discussed in Chap. 13.

Prussian blue, which has a dark blue-black color, can be both reduced and oxidized electrochemically. Reduction occurs at a potential about 195 mV positive of the SCE potential, and thus about 678 mV positive of the reversible hydrogen potential. The reduction product is white, and is generally called "Everitt's salt," although it is sometimes also designated as "Prussian white." As already mentioned, its composition can nominally be described as $K_2FeFe(CN)_6$ when K^+ ions are in the A sites.

Oxidation of Prussian blue occurs when the potential is made more positive. This occurs at about 870 mV vs. the SCE reference, and thus 1.348 mV positive of the reversible hydrogen potential. The product is only lightly colored, and is generally called "Berlin green." Its composition can be nominally described as $FeFe(CN)_6$.

A second oxidation reaction, involving the insertion of anions into the A position, is sometimes found at about 1,100 mV vs. the SCE potential, where a yellow product called "Prussian yellow" is formed. This material is unstable in water, as would be expected from its potential, some 1.8 V positive of the reversible hydrogen potential. Its nominal compositions can be written as $FeFe(CN)_6A_x$.

All of these materials have essentially the same basic cubic unit cell, with a lattice parameter of about 10.2 A. Although incorporated water is not included in these nominal compositions, these materials are generally found to contain substantial amounts of water of hydration around the A species.

Electrochemical experiments have often been made using cyclic voltammetry. A typical example is shown in Fig. 22.11. It is seen that there are reversible current peaks in two quite different potential regions, relating to the reduction and oxidation reactions described above. The second oxidation reaction at even more positive potentials is not shown in that figure because the scan rate was rather low and the potential was not increased sufficiently for it to be seen. Another voltammogram is shown in Fig. 22.12 under conditions that made it possible to see the formation of the chemically unstable Prussian yellow at more positive potentials.

The critical potentials in the Prussian blue system are shown schematically in Fig. 22.13. One can translate the semi-quantitative dynamic data obtained from cyclic voltammetry experiments into the results that would be expected if electrochemical potential spectroscopy experiments were performed. Likewise, they could be expressed as an equilibrium titration curve, as indicated schematically in

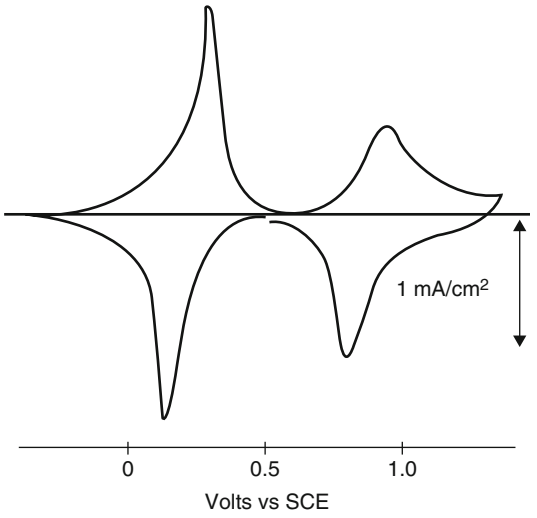

Fig. 22.11 Typical voltammogram of Prussian blue, After [34]

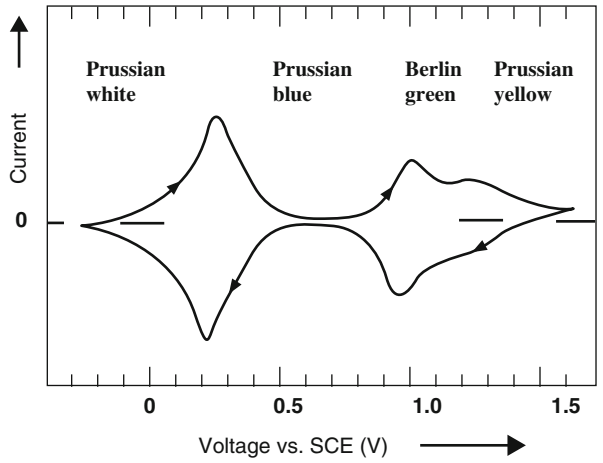

Fig. 22.12 Voltammogram that also shows the reaction to form Prussian yellow at more positive potentials

Fig. 22.14. In this case the formation of Prussian yellow will not be included, as it is not stable in water, as indicated earlier.

Experiments of this type provide more quantitative information about the potentials at which the reduction and oxidation reactions take place than can be obtained from the more common dynamic cyclic voltammetry experiments. However, in the case of Prussian blue, the kinetics of the relevant phenomena are so fast that there is not much difference between the information obtained from dynamic and static experiments.

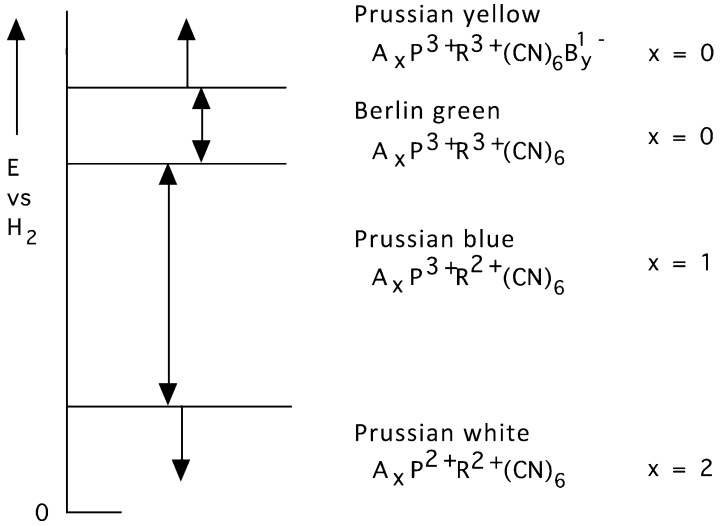

Fig. 22.13 Schematic representation of the potentials at which the several reactions occur in Prussian blue

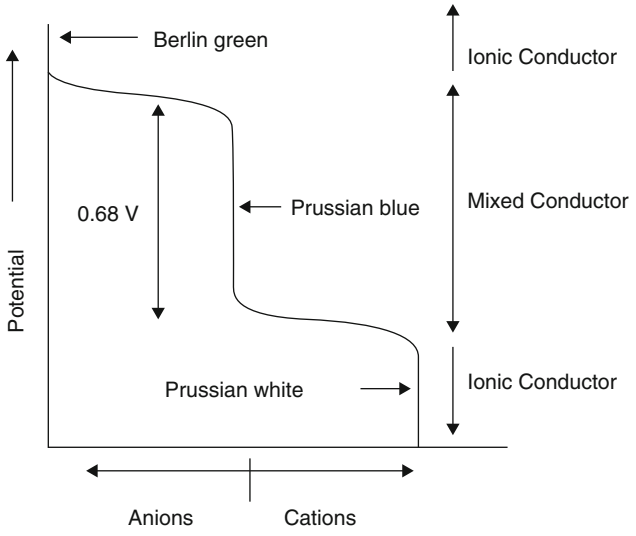

Fig. 22.14 Schematic equilibrium electrochemical titration curve for the Prussian blue system

Table 22.1 Assumed radii of hydrated cations

Cation	Radii (A)
Li^+	2.37
Na^+	1.83
K^+	1.25
NH_4^+	1.25
Rb^+	1.18
Cs^+	1.19
Ba^{2+}	2.88

22.6.4 Various Cations Can Occupy the A Sites in the Prussian Blue Structure

A number of different cations can be present in the A positions in the hexacyanometallate structure. Monovalent examples include Li^+, Na^+, K^+, NH_4^+, Rb^+, and Cs^+ ions. The ability of these various ions to reversibly enter the structure has been interpreted in terms of their size when hydrated. These are shown in Table 22.1 below, which also includes the hydrated divalent Ba^{2+} ion.

The hard-sphere model of the Prussian blue structure has an intercell window radius of 1.6 A. Thus it is expected that it would be difficult for cations with hydrated radii greater than this value to readily move into and out of the structure. This corresponds to what is found experimentally from dynamic electrochemical measurements [25].

Hydrated NH_4^+ and Rb^+ can be cycled many times, although their insertion/extraction kinetics are significantly slower than hydrated K^+ ions. Both smaller (Cs^+) and larger (Li^+ and Na^+) hydrates showed much more restricted behavior.

In non aqueous electrolytes where the mobile cations are not hydrated these insertion reactions occur much more slowly and are not so interesting from a practical point of view. This is typical of the ionic transport behavior when the mobile species is relatively small in comparison to the host structure through which it moves.

22.6.5 Batteries with Prussian Blue Electrodes

There has been interest in the use of materials in the Prussian blue family as electrodes in batteries for some time. In 1985 V.D. Neff [35] made a cell with Everitt's salt (or "Prussian white") on the negative side, and "Prussian yellow" on the positive side, which gave an initial voltage of 0.93 V in an acid solution of 1 N K_2SO_4. The voltage across this configuration gradually decayed to 0.68 V, due to the instability of Prussian yellow in water, and its replacement by "Berlin green." Two years later Honda and Hayashi [36] showed that a rechargeable battery could

be produced from Prussian blue family materials using Nafion as a solid electrolyte. In this case, a stable output voltage of 0.68 V was also observed. Upon discharge, both electrode materials change to Prussian blue, and the voltage dropped to zero in those cells.

There has been a considerable amount of work done recently on the development of practical batteries based upon materials in the Prussian blue family.

An interesting group of materials with such open framework crystal structures are the mixed-valence hexacyanoferrates, which are often called ferrocyanides. They readily intercalate a number of different hydrated ions, including Li^+, Na^+, K^+, and NH_4^+ from aqueous electrolytes [37–41].

Prussian Blue, the oldest and most studied material of this type, has the basic hexacyanometalate metal-organic framework. Materials with this structure may be described in terms of the general formula $A_xPR(CN)_6$. Nitrogen-coordinated transition metal cations (P) and hexacyanometalate complexes ($R(CN)_6$) form a face-centered cubic open framework containing large interstitial A sites, which may be partially, or fully, occupied by a number of different, generally hydrated, ions in this structure. The ionic occupancy of these A sites may vary, with corresponding valence changes in one or both of the P and R species.

As mentioned earlier, the high electrochemical reversibility of materials in this family has been known for some time. For example, the robust framework structure of Prussian Blue and its analogues has been shown to allow thin film electrochromic devices to operate for 10^5 to 10^7 cycles at high cycling rates [32, 33].

These relatively inexpensive materials possess remarkable electrochemical performance, operate in safe, inexpensive aqueous electrolytes, and may be synthesized using bulk processes at modest temperatures. Hence, they are especially attractive for use in large-scale stationary batteries to provide storage capacity for use with the electrical power grid.

Materials in the Prussian Blue family can be easily synthesized by the use of simple ambient temperature precipitation from aqueous solutions. Two examples are copper hexacyanoferrate, (CuHCF) [38] and nickel hexacyanoferrate (NiHCF) [39]. Both CuHCF and NiHCF can readily be synthesized as nanopowders in this way. Simultaneous, dropwise addition of 40 mM copper or nickel nitrate, and 20 mM potassium ferricyanide into deionized water produces controlled co-precipitation of uniform fine particles of either CuHCF or NiHCF. The synthesis of CuHCF is readily done at room temperature, while the synthesis of NiHCF is performed at 70 ° C. These solid products are then filtered, washed with water, and dried in vacuum at room temperature. The products can have a high degree of crystallinity.

Several different common alkali metal ions can be reversibly inserted into these materials from aqueous electrolytes, Li^+, Na^+, K^+, and NH_4^+, and they can be readily synthesized as nanopowders. In each case, the crystallographic lattice parameter varies only slightly, and linearly, with the concentration of the inserted ions.

However, the stiffness of the structure and the size of the interstitial sites result in only minor dimensional changes when the concentrations of the inserted ions are modified during charging and discharging. This is an important factor, for it leads to the unusually long cycle lives observed in this family of materials.

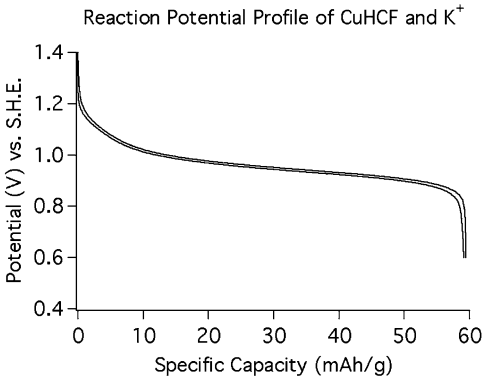

Fig. 22.15 Variation of the potential during the discharge and recharge of (CuHCF) at a 0.83 C rate [38]

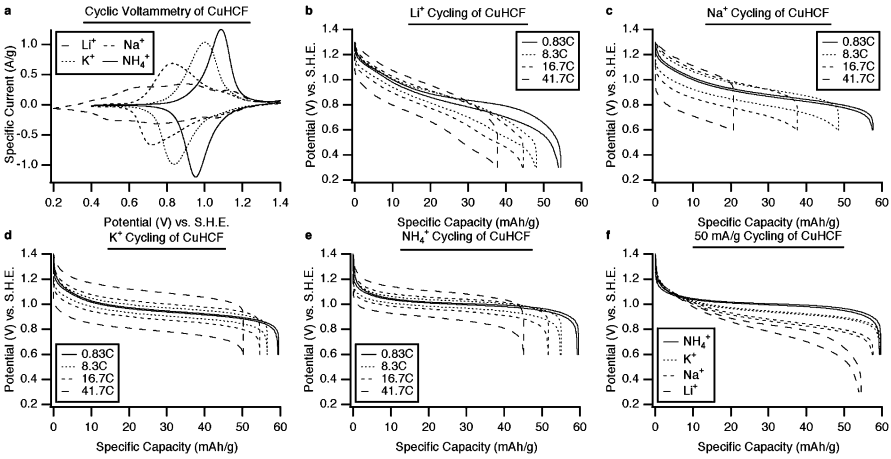

Fig. 22.16 Electrochemical performance of CuHCF. (**a**) Cyclic voltammetry of CuHCF with Li^+, Na^+, K^+, and NH_4^+ ions, and (**b**) through (**e**): The potential profiles of CuHCF during galvanostatic cycling of Li^+, Na^+, K^+, and NH_4^+, respectively, at several current densities. (**f**) The potential profiles of CuHCF during galvanostatic cycling of Li^+, Na^+, K^+, and NH_4^+, at 50 mA/g (0.83C) [38]

As an example, potassium ions can be reversibly reacted with $KCuFe^{3+}(CN)_6$ (CuHCF) to produce $K_2CuFe^{2+}(CN)_6$ [38]. The discharge–recharge data at a rate of 0.83C for this case are shown in Fig. 22.15. It can be seen that this behavior is very unusual. There is very, very little hysteresis, so that the energy absorbed per cycle is very small. The shape of the curve is what is expected for a single-phase solid solution reaction.

Materials in this family have shown remarkable cycling behavior: for they can be fully charged and recharged at unusually high rates for a very large number of cycles. This is illustrated in Fig. 22.16 for the case of CuHCF, and in Fig. 22.17 for the analogous NiHCF [39].

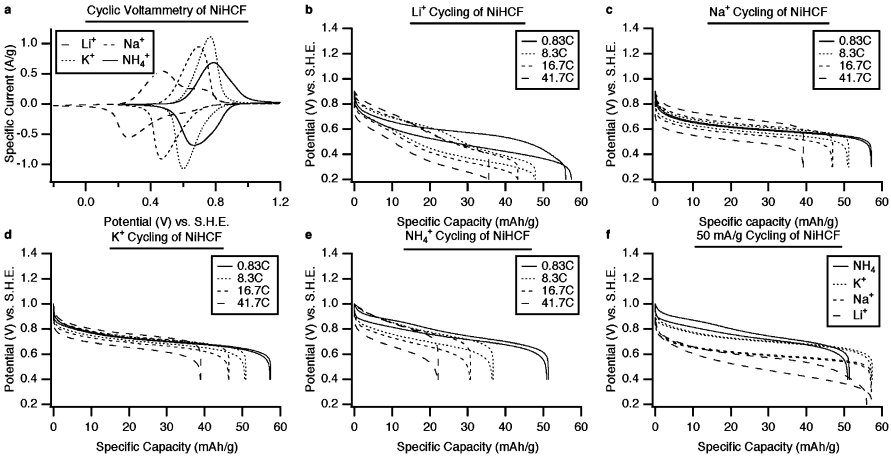

Fig. 22.17 Electrochemical performance of NiHCF. Cyclic voltammetry of NiHCF with Li^+, Na^+, K^+, and NH_4^+ ions, and (**b**) through (**e**): The potential profiles of NiHCF during galvanostatic cycling of Li^+, Na^+, K^+, and NH_4^+, respectively, at several current densities. (**f**) The potential profiles of NiHCF during galvanostatic cycling of Li^+, Na^+, K^+, and NH_4^+, at 50 mA/g (0.83C) [39]

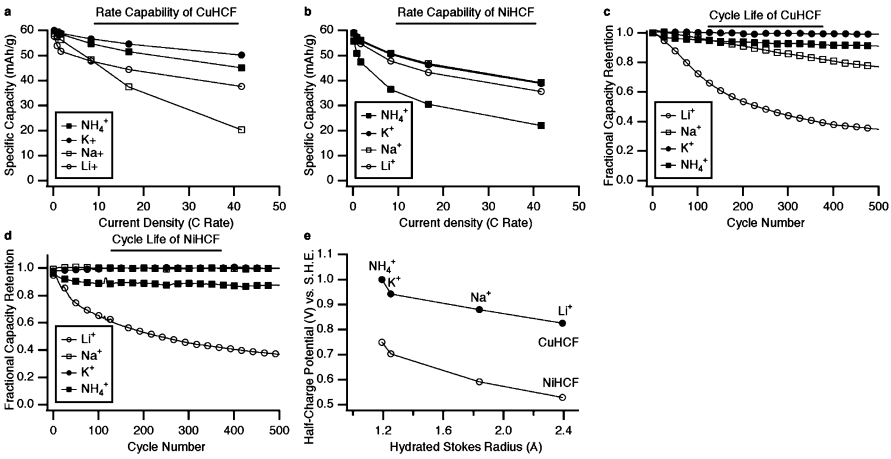

Fig. 22.18 Rate capability, cycle life, and effect of insertion ion size of CuHCF and NiHCF. (**a**) and (**b**) The capacity retention of CuHCF and NiHCF at various current densities. (**c**) and (**d**) The cycle life of CuHCF and NiHCF during cycling of Li^+, Na^+, K^+, and NH_4^+, and (**e**) The reaction potentials CuHCF and NiHCF as functions of the Stokes radius of the insertion ion [40]

The rate capability and cycle life, as well as the influence of the identity of the inserted ion upon the half-charge potential are illustrated in Fig. 22.18 [40].

22.6.6 Investigations of the Use of Polyvalent Prussian Blue Electrodes in Aqueous Systems

Because of the possibility that the capacity of Prussian Blue could be increased if the inserted species could carry more than one charge, experiments have been reported [42] in which the insertion of alkaline earth divalent cations : Mg^{2+}, Ca^{2+}, Sr^{2+} and Ba^{2+}, into nickel hexacyanoferrate was investigated.

There has also been some recent work on the investigation of the insertion of divalent and trivalent ions into copper and nickel hexacyanoferrate [43–46].

Water molecules, which typically are present in such materials, screen the larger charge. Such groups, rather than single ions, may move into the structure, replacing one of the Fe ions in the normal ferrocyanides.

22.6.7 Work Toward the Commercialization of Aqueous Electrolyte Batteries Containing Prussian Blue Electrodes

Work on the development of commercial batteries based upon the use of materials in the Prussian Blue family is currently being pursued by the firm Alveo Energy, which Colin Wessells formed after the completion of his PhD program at Stanford University.

22.6.8 Prussian Blue Electrodes in Organic Electrolytes

Although the discussion of the Prussian blue family of materials here has thus far involved their behavior in aqueous electrolytes, they can also be used in appropriate organic electrolytes. The incentive for this work is the fact that some organic electrolytes can be stable over significantly greater ranges of potential than aqueous electrolytes. This can lead to batteries with substantially greater voltages than is possible with aqueous electrolytes.

As described elsewhere in this book, lithium is the typical anode material in current organic electrolyte rechargeable batteries, and it readily inserts into typical current positive electrode materials. However, it cannot be reversibly inserted into the Prussian blue structure from aqueous electrolytes, due to the large size of solvated lithium ions. As a result, lithium insertion and extraction in the Prussian blue family of materials in aqueous electrolytes is not considered practical. Instead, the other alkali metal ions, which have smaller solvation shells, are more favorable.

The first experiments on the behavior of Prussian blue materials in organic electrolytes were reported by A. Eftekhari [45]. He used Prussian blue as a cathode, with a potassium anode, in an EC/EMC electrolyte containing 1 M KBF_4.

The behavior is illustrated in Fig. 22.19.

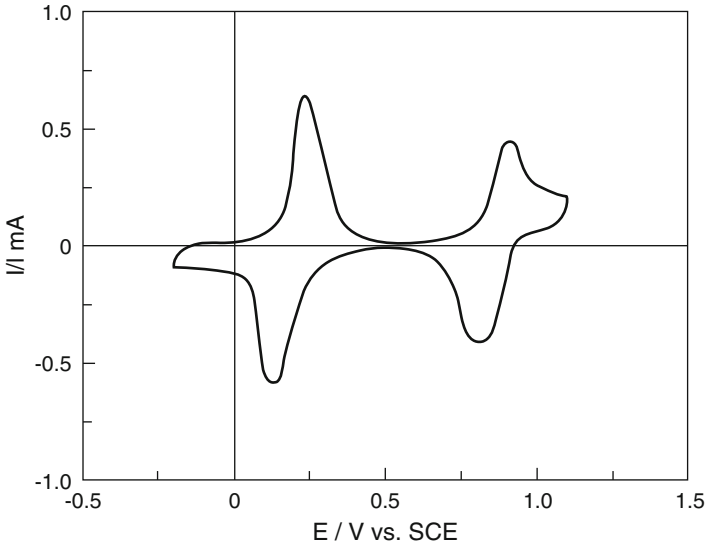

Fig. 22.19 Cyclic voltammetric behavior of a Prussian blue electrode in a nonaqueous electrolyte at a scan rate of 10 mV/s. From ref. [46]

In organic electrolytes the potential of potassium is only 0.12 V positive of that of lithium, whereas the potential of sodium is 0.32 V positive of lithium. As a result, potassium negative electrode cells have greater voltages than equivalent sodium cells. Potassium is also more attractive for kinetic reasons, for it has a significantly smaller solvation shell than sodium. This leads to quite favorable cycling behavior in nonaqueous electrolytes.

The difference between the cyclability of Prussian blue containing either potassium or lithium in a nonaqueous electrolyte is shown in Fig. 22.20, and the relatively minor change in the capacity of a potassium-containing cell after 500 cycles is illustrated in Fig. 22.21.

Investigations in the Goodenough laboratory at the University of Texas have been reported more recently on the behavior of Prussian blue electrodes with compositions $KMFe(CN)_6$ in which the M species was Mn, Fe, Co, Ni, Cu, and Zn. Although these materials initially contained potassium, they were cycled in an organic electrolyte containing equal amounts of EC and DEC and 1 M NaClO4 using sodium as the anode material [47]. They were able to obtain a reversible capacity of over 70 mAh/g in the range of 2.0 to 4.0 volts vs. Na at rates of C/20 in some cases (Fig. 22.22).

Subsequent work in that laboratory [47] involved the investigation of a sodium-only Mn–Fe ferrocyanide using a carbonate electrolyte. Two different compositions resulted in slightly different capacities. In Fig. 22.23 it is seen that these materials still showed appreciable capacities when discharged at very high rates in organic electrolytes.

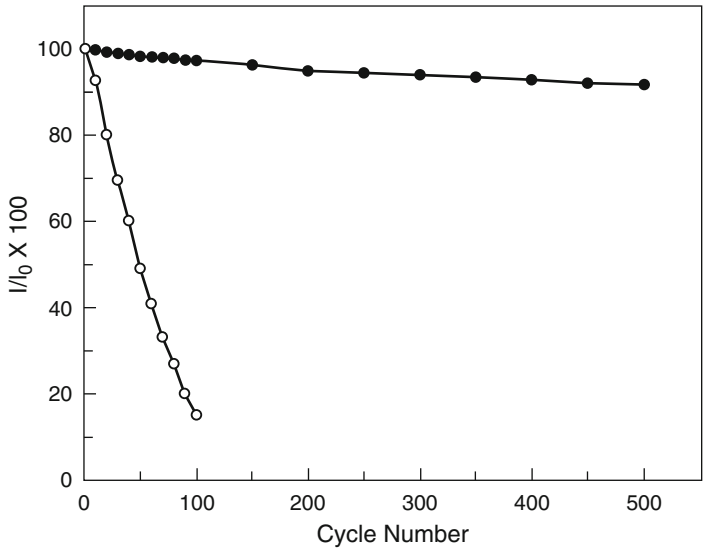

Fig. 22.20 Difference in the cyclability of lithium and potassium in nonaqueous solutions of KBF_4 and $LiBF_4$. The *open circles* are data for lithium, and the *solid circles* for potassium, insertion/extraction. From ref. [45]

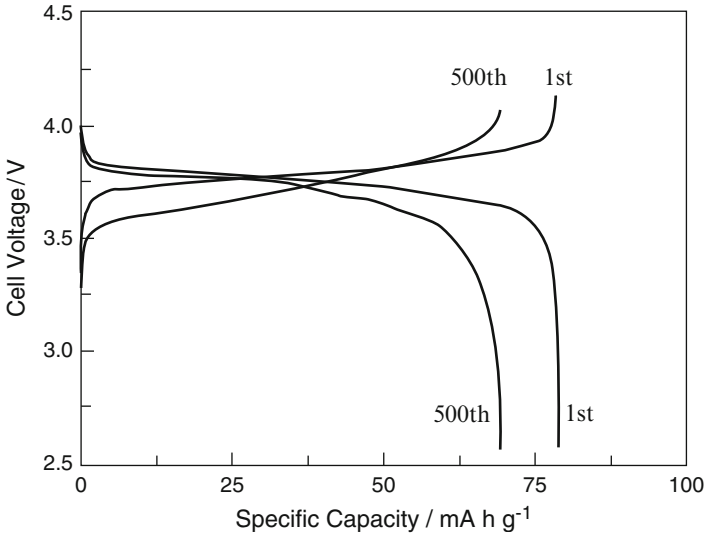

Fig. 22.21 Relatively small change in the charge–discharge characteristics of a Prussian blue cell with a potassium anode and a Prussian blue cathode at a C/10 rate after 500 cycles**.** From ref. [45]

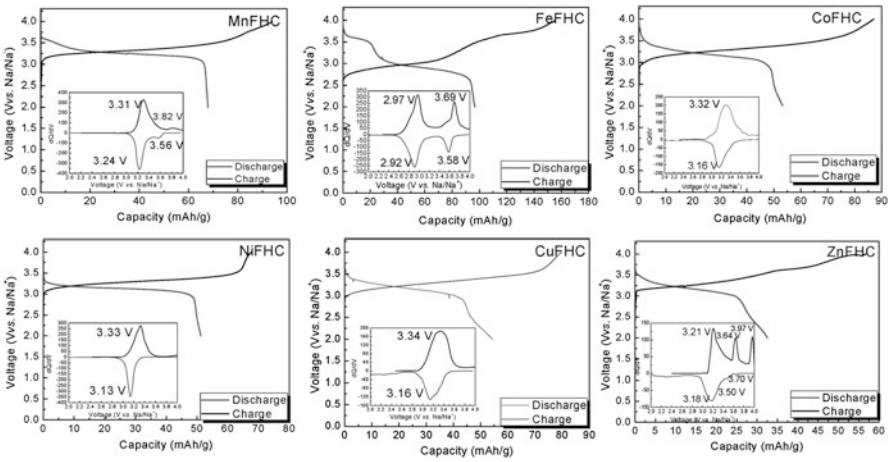

Fig. 22.22 Charge–discharge data for Prussian Blue electrodes with several different compositions in an organic electrolyte [46]

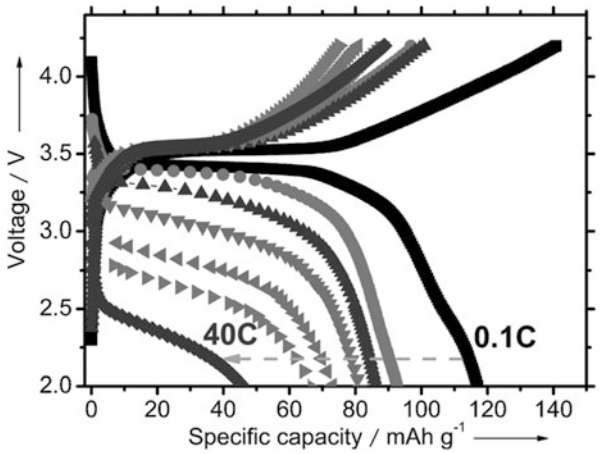

Fig. 22.23 Behavior of Mn-Fe ferrocyanide electrodes at high rates (after [47])

22.7 A New Class of Composite Anodes

The simplest way to make a useful cell with these attractive Prussian blue cathode materials would be to use large surface area activated carbon (AC) as the anode. However, when using such a capacitive anode the cell voltage varies significantly with the state of charge. This is illustrated in Fig. 22.24.

To avoid this disadvantage, a new class of anodes that are compatible with the open framework CuHCF and NiHCF materials in aqueous electrolytes have been developed [48–50]. These anodes are based on a hybrid microstructure that operates

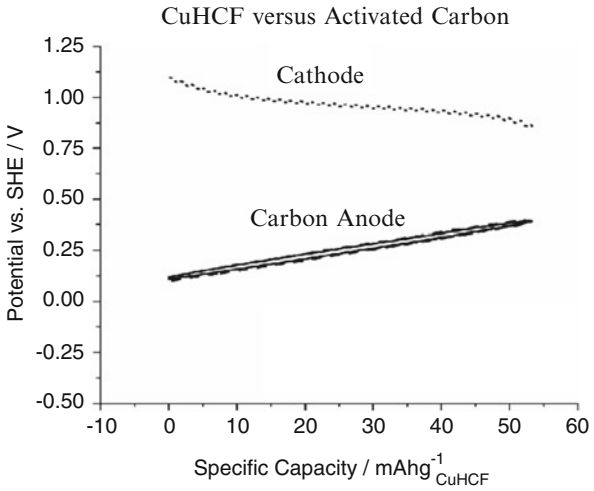

Fig. 22.24 Variation of the potential during galvanic cycling of a cell with CuHCF and activated carbon electrodes at a 1 C rate [48]

by a new concept: by combining an electrode material (polypyrrole, PPy) that undergoes a faradaic anion doping/dedoping reaction at a fixed potential with a capacitive electrode (activated carbon), the potential of the entire electrode can be controlled.

Fundamentally different from either traditional capacitive or active battery electrodes, this new hybrid electrode has the high rate capability of a capacitor, but with the well-defined electrochemical potential of a battery electrode. It has an attractive open circuit potential (OCP), tunable to −0.2 V versus SHE, a shallow charge–discharge profile and leads to no cell self-discharge. Furthermore, a full cell with this hybrid anode and a CuHCF cathode has shown performance that is promising for grid-scale and other stationary storage applications: high power and energy efficiency, and a lifetime of thousands of cycles.

It has been shown that the potential of this type of negative electrode can be modified by reducing the polypyrrole with $NaBH_4$. This increases the voltage of the cell, as illustrated in Fig. 22.25.

The resultant properties of the full cell at a 10 C rate are illustrated in Fig. 22.26.

The negligible variation of the capacity and Coulombic efficiency with cycling is illustrated in Fig. 22.27. It can be seen that there is no measurable capacity loss after 1,000 cycles at the 10 C rate.

Full cells with this ferrocyanide/stabilized carbon electrode combination have also been shown to have very attractive kinetic properties. The influence of the charge–discharge rate upon the cell voltage and capacity is illustrated in Fig. 22.28.

The energy efficiency and capacity retention during cycling at different rates are shown in Fig. 22.29.

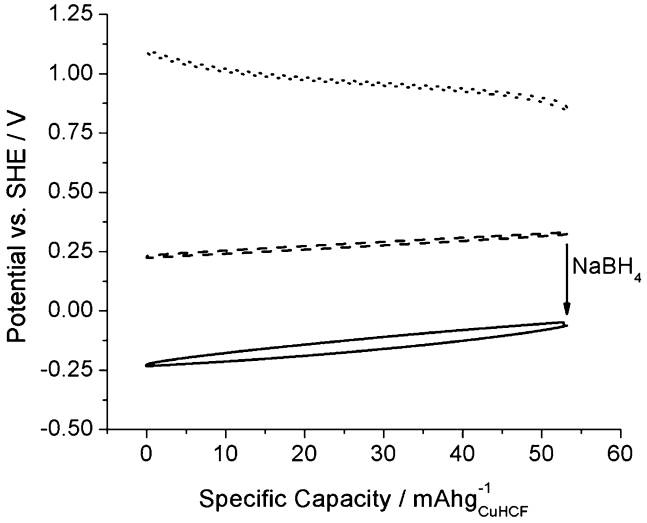

Fig. 22.25 Variation of the potential during galvanic cycling of a cell with CuHCF and activated carbon electrodes containing 10 % polypyrrole at a 1 C rate [48]

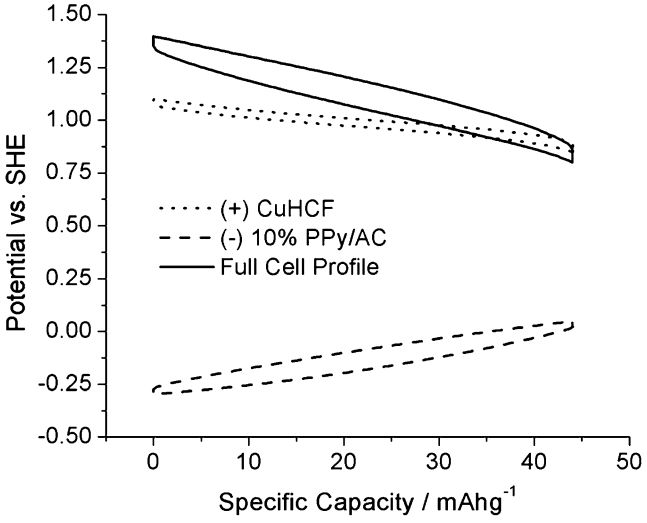

Fig. 22.26 Potential profiles of copper hexacyanoferrite (CuHCF) positive electrode, 10 % polypyrrole (PPY)/activated carbon (AC) negative electrode and full cell voltage measured at rate of 10C [48]

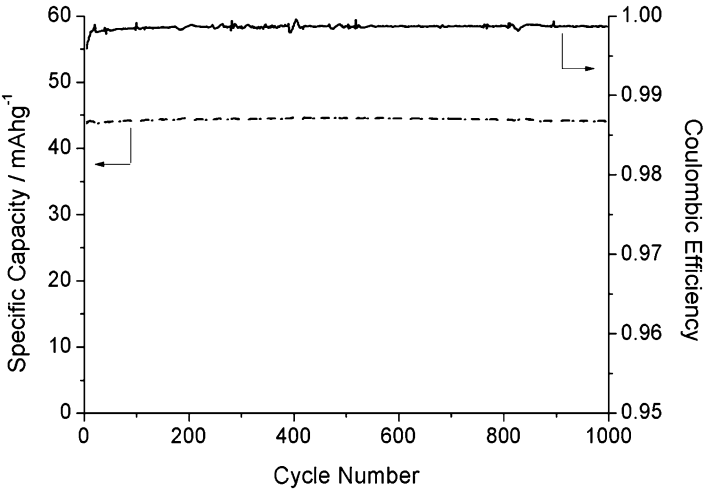

Fig. 22.27 Variation of the specific capacity and Coulombic efficiency with cycle number [48]

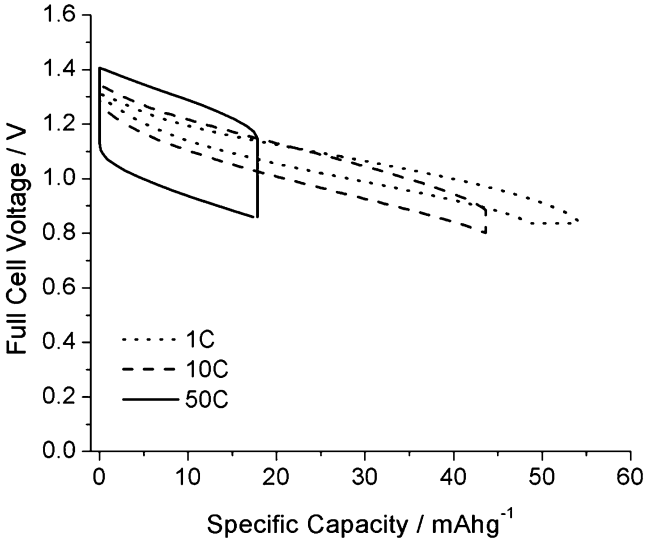

Fig. 22.28 Full cell potential profiles at 1 C, 10 C, and 50 C rates [48]

22.8 An Alternative, Extension of the Stability Range of Aqueous Electrolytes

Although the stability range of aqueous electrolytes is often quoted as 1.23 V, based upon the Gibbs free energy of formation of H_2O, that value is actually only applicable to pure water at ambient temperature. If the activity of water at the

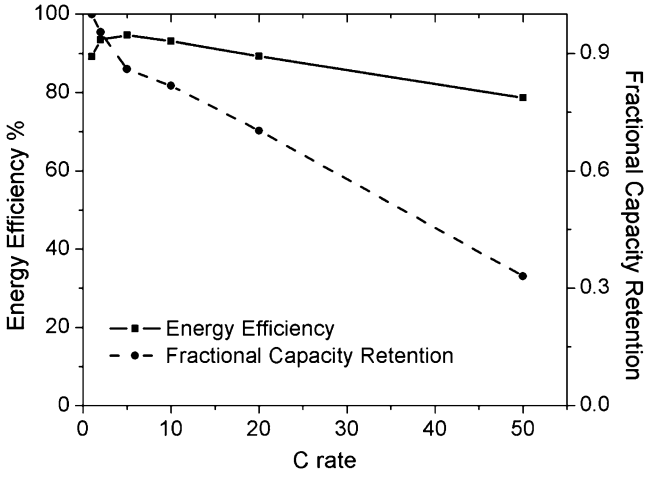

Fig. 22.29 Energy efficiency and fractional capacity retention as a function of the C rate [48]

electrochemical interface is decreased, the stability range can be appreciably extended, allowing larger cell voltages. This can be an attractive alternative to the use of organic electrolytes, for aqueous electrolytes are inherently nonflammable, and can have significantly higher ionic conductivity, and appreciably lower costs than the common organic electrolytes.

There are two general ways in which this can be accomplished. One is to have an additional electrolyte present that acts in series with the aqueous electrolyte. As mentioned in Chap. 18, the potential of a Zn electrode in aqueous batteries is 0.43 V negative of the theoretical potential for the evolution of hydrogen, due to the presence of a thin ionically-conducting, but electronically-insulating layer of ZnO on its surface. Similarly, as shown in Chap. 17, lead-acid cells typically operate at voltages between 2.0 and 2.15 V, and hydrogen and oxygen do not evolve until 2.4 V because of a dense corrosion film of electronically-insulating, but ionically-conducting $PbSO_4$. Metal hydride/nickel cells operate at 1.34 V, and oxygen evolution does not start until 1.44 V, due to the formation of an electrically-conducting, but proton-conducting layer of $Ni(OH)_2$ in contact with the electrolyte, as discussed in Chap. 19. In all of these cases the operating voltage can exceed the thermodynamic stability range of pure water.

A second situation that can also lead to the use of larger cell voltages is the reduction of the chemical potential of water by dissolving other species into it. Concentrated salt solutions can have practical stability ranges significantly greater than that of pure water. This is because a large fraction of the water molecules in solution participate in the hydration shells of the various ions, greatly reducing the mobility of the protons and hydroxyl ions present in the water. This is a kinetic, rather than thermodynamic, effect, but it reduces the effective chemical activity of the water, and extends its range of practical stability.

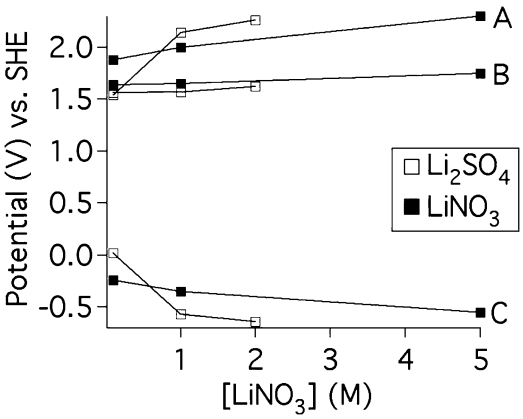

Fig. 22.30 (**A**) full cell voltage, (**B**) working electrode and (**C**) counter electrode potentials for Li_2SO_4 and $LiNO_3$ as a function of their concentrations at a current density of 50 μA/cm^2 [51]

The resultant low leakage current densities across concentrated aqueous salt solutions allow the practical use of larger cell voltages than is possible with pure water. At low leakage current densities, e.g.10 μA/cm^2, such electrolytes can have useful voltage windows of about 2 V. If leakage current densities up to 50 μA/cm^2 can be tolerated, the useful cell voltage can be up to 2.3 V.

If the applied voltage is above the equilibrium stability limit of an aqueous electrolyte, a leakage current will be present that will act to produce self-discharge of any aqueous electrolyte battery. The magnitude of the self-discharge rate depends upon the relationship between the electrode potentials and the stability limits of the electrolyte.

As the span of the useful electrolyte window depends upon the current density, its practical value depends upon the allowable rate of self-discharge. Given the proper choice of electrode and electrolyte materials, aqueous electrolyte batteries may successfully operate at voltages well above the nominal thermodynamic stability range of pure water, 1.23 V.

The location of the electrolytic stability range of pure water depends upon the pH, varying approximately 0.059 V per pH unit.

Concentrated $LiNO_3$ and Li_2SO_4 have been used in aqueous lithium battery experiments [51, 52]. They have neutral values of pH and have stability ranges that vary with the salt concentration. They have a stability range greater than 2.3 V at a leakage current density of 50 μA/cm^2, as shown in Fig. 22.30.

Experiments have shown that there is a linear relationship between the potential stability range and the logarithm of the current density in both of these concentrated salt solutions. In Fig 22.31 it can be seen that the total stability range of water with 5 M $LiNO_3$ is slightly greater than that with 2 M Li_2SO_4 at all current densities.

Similar experiments were performed with a number of other salts, which also showed that the practical stability range can be extended appreciably beyond the value for pure water.

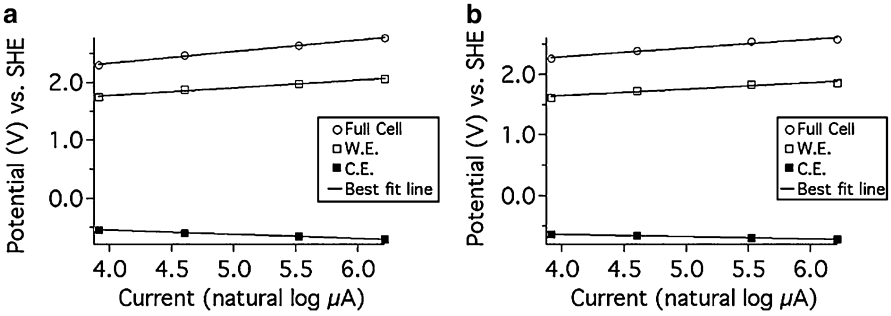

Fig. 22.31 Semi-logarithmic plots of the full cell voltage, and working (W.E.) and counter electrode (C.E.) potentials of 5 M $LiNO_3$ (**a**) and 2 M Li_2SO_4 (**b**) as a function of current density [51]

All these electrolytes exhibited minor values of leakage current, which varied with the applied voltage. As mentioned above, a linear relationship was found between the logarithm of the current and the voltage. This is what is expected if there is minority electron or hole leakage through a liquid electrolyte [53, 54] and is also observed in experiments on minority electronic transport in solid electrolytes [55].

This behavior is also consistent with the empirical Tafel approximation of the general Butler-Volmer "activated complex" model of current transport across the "electron-transfer-limited region" of the electrolyte/electrode interface.

During operation, the voltages of batteries generally decrease from their maximum values as they are discharged. The result is that their rates of self-discharge also decrease. Thus this is often not a serious problem with high voltage aqueous cells.

22.9 Batteries With Liquid Electrodes

In discussions of batteries it is commonly assumed that they have solid electrodes and a liquid electrolyte. One exception to this is discussed in Chap. 12, however, the "Zebra" cell. In that case one of the electrodes is liquid sodium, and the other is solid $NiCl_2$ that is permeated by liquid $NaAlCl_4$. That arrangement could be described as a L/S/L,S configuration.

In this chapter some other battery types are discussed in which one or both of the electrode reactants are liquids.

22.10 Sodium/Sulfur Batteries

A type of battery that is beginning to be used for storing energy in large scale systems is the so-called *sodium/sulfur battery* that operates at 300–350 °C. This electrochemical system is best described as a Na/Na_xS cell. These batteries are different

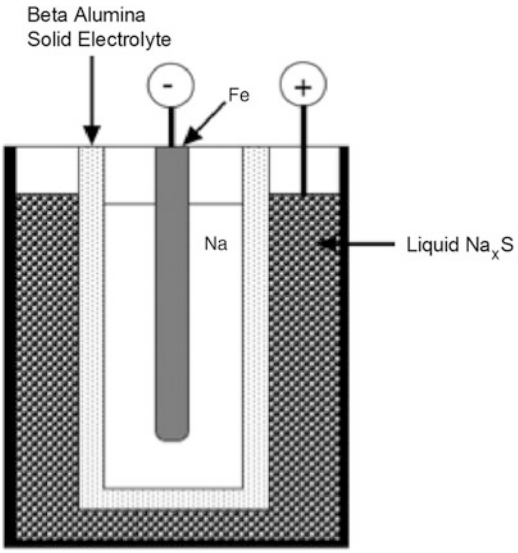

Fig. 22.32 Schematic view of Na/Na_xS cell

from the common systems that most people are familiar with, for the electrodes are liquids, instead of solids, and the electrolyte is a solid sodium ion-conducting ceramic solid, $NaAl_{11}O_{17}$, called *sodium beta alumina*. This is thus a L/S/L configuration, which is the inverse of the conventional S/L/S, arrangement.

The sodium ion conductivity in this ceramic material, discovered by Yao and Kummer, is remarkably high at the operating temperature [53, 54, 56], about 4 Ω cm at 350 °C. The possibility that this material could be used to construct the revolutionary sodium/sulfur battery was soon pointed out by Weber and Kummer [55]. A general reference that contains a lot of information about sodium/sulfur cells is [57].

In this case the negative electrode is molten sodium, and the positive electrode is the product of the reaction of sodium with liquid sulfur. Thus the basic reaction can be written as

$$x\mathrm{Na} + \mathrm{S} = \mathrm{Na}_x\mathrm{S} \tag{22.1}$$

The general construction of such batteries is shown schematically in Fig. 22.32.

Sodium from the negative electrode passes through the surrounding solid beta alumina cylinder, and reacts with a liquid solution of sodium in sulfur, Na_xS. This liquid, which is not a good electronic conductor, is contained in a porous carbon "sponge" to provide electrical contact to the positive current collector.

The capacity is determined by the composition range of this sodium-sulfur liquid phase. The relevant portion of the Na-S phase diagram is shown in Fig. 22.33. It is seen that at about 300 °C only a relatively small amount of sodium can be dissolved in liquid sulfur. When this concentration is exceeded, a second liquid phase, with a composition of about 78 atomic percent Na, is nucleated. This has a composition that extends to roughly $Na_{0.4}S$. As more sodium is added the overall composition

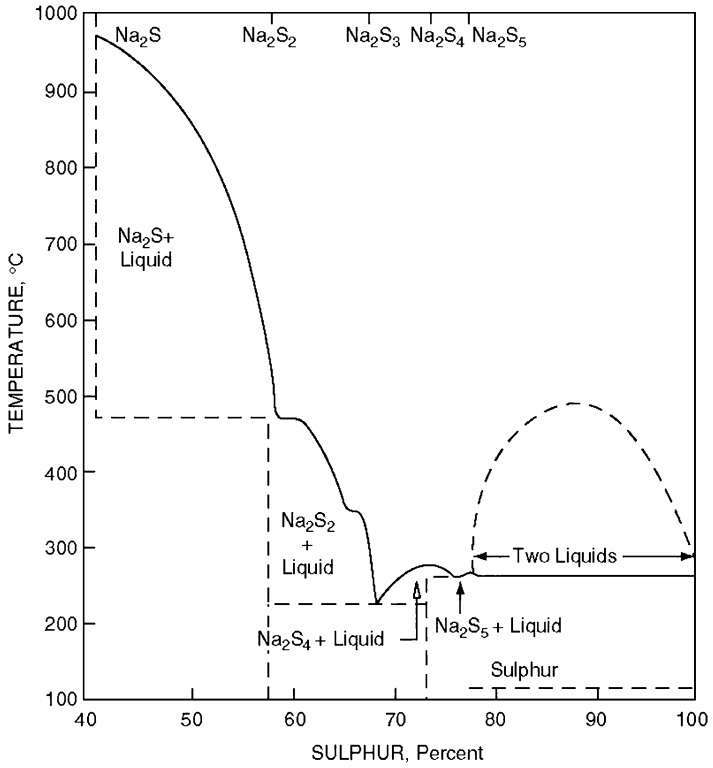

Fig. 22.33 Part of the sodium-sulfur phase diagram

traverses the two-phase region, and the amount of this liquid phase increases relative to the amount of the sulfur-rich liquid phase. Thus a potential plateau is expected over this two-phase composition range. When the sodium concentration exceeds that corresponding to about $Na_{0.4}S$ the overall composition moves into a single-phase liquid range, and thus the potential varies with the composition. The maximum amount of sodium that can be used in this electrode corresponds roughly to $Na_{0.67}S$.

At higher sodium concentrations a solid second phase begins to form from the liquid solution. This tends to form at the interface between the solid electrolyte and the liquid electrode, and prevents the ingress of more sodium, thus blocking further reaction.

The potential of the elemental sodium in the negative electrode is constant, independent of the amount of sodium present. The potential of the positive electrode, and thus the voltage of the cell, changes as the sodium concentration varies by its transport across the cell. The variation of the potential of the positive electrode with its composition is shown in Fig. 22.34.

Early work in both the United States and Europe on this type of cell was aimed toward its potential use for vehicle propulsion. In that case, safety is especially

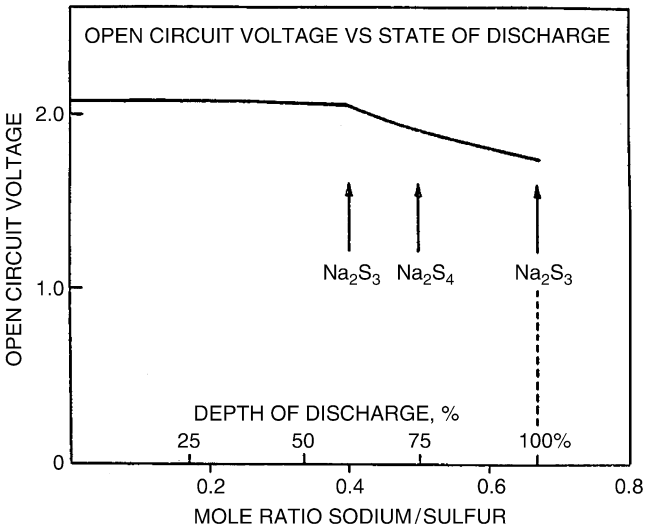

Fig. 22.34 Voltage versus pure sodium as a function of composition

important, and extensive testing related to the use of these cells in vehicles under crash conditions was performed in Europe in 1990s. The results of these tests were discouraging, and all of those development programs were discontinued.

On the other hand, activities in Japan were aimed at a different application, utility power storage, where they can be kept in a protective environment so that safety considerations can be minimized. A large effort was undertaken by a consortium of NGK Insulators and Tokyo Power (TEPCO) in 1983, and after extensive large scale testing, large sodium/sulfur cells became commercially available in 2000.

The large individual cells, roughly the size of a baseball bat, are enclosed in steel casings for safety reasons, and they can be arranged into parallel and series groups in order to provide the required voltage and capacities.

However, a major fire occurred in a large sodium/sulfur battery system in Tsukuba, Japan in September, 2011. It involved the leakage of hot liquids from one cell into a number of nearby ones, and then propagated into a serious problem for a large system, which, fortunately, was in an outside location. This caused widespread concern about the safety of even stationary sodium/sulfur battery systems, and NGK asked that all large batteries of this type be shutdown until the cause of the problem was identified, and a solution developed that would prevent a recurrence of this problem. This was done, and a number of design changes were made, including the installation of fuses on all individual cells.

Modified systems with power values up to 6 MW at 6.6. kV are now being produced and used in Japan. This technology is also beginning to be installed in the United States, with facilities currently up to a 1 MW size.

22.11 Flow Batteries

22.11.1 Introduction

Except for the Na/Na_xS cell, and the Zebra cell, that was discussed briefly in Chap. 12, all of the electrochemical cells that are generally considered have electrodes that are solids. In those two cases liquid electrodes can be used because the electrolyte is a solid, resulting in an L/S/L configuration.

There is another group of cells that have liquid electrode reactants, although their electrode structures contain porous solid current collectors. These are generally called "flow batteries," since the liquid reactant is stored in tanks and is pumped (flows) through the cell part of the electrochemical system. Thus such systems can also be considered to be rechargeable fuel cells.

Early work on flowing electrode systems was done by Lawrence Thaller at the NASA laboratory in Ohio during the 1970s. He used an iron–chromium electrochemical combination. The effective valence of iron changed from Fe^{2+}/Fe^{3+}, and that of chromium from Cr^{2+}/Cr^{3+} at a nominal voltage of 1.18 V. However, these early cells suffered from severe cross-contamination, which resulted in rapid capacity decay.

This problem can be mitigated somewhat by using a premixed electrolyte on both sides [58]. This general approach is currently being pursued by the firm Deeya Energy, Inc.

Following this early work a number of chemical systems have been explored, and in some cases rather fully developed. However, most of them have not been commercially successful to date. As seen below, this could well change in the near future. A total of 13 programs that involve development efforts on various types of flow batteries are currently receiving financial support from the US government agency ARPA-E.

The general physical arrangement is shown in Fig. 22.35, whereas the configuration of the cell portion of the system is shown schematically in Fig. 22.36.

It can be seen that this is also a type of L/S/L configuration. The electrolyte is a proton-conducting solid polymer, and the electrode reactants are liquids on its two sides. In the Zebra cell the reactants are both electronically-conducting, whereas in the flow cells the electrode reactants are ionic aqueous solutions that are electronic insulators. In order to get around this problem and provide electronic contact to an external electrical circuit, the liquid reactants permeate an electronically conducting graphite felt. This felt provides contact, both to the polymer electrolyte and to a graphite current collector.

The electrode reactants are typically acidic, e.g., 2 M H_2SO_4 aqueous solutions of ions that can undergo redox reactions. The function of the polymer electrolyte is to transport protons from one side to the other, thus changing the pH and charges on the dissolved redox ions.

An important difference from the Na/Na_xS and Zebra cells is that the reactant materials, the redox ion solutions, can be pumped into and out of the electrode

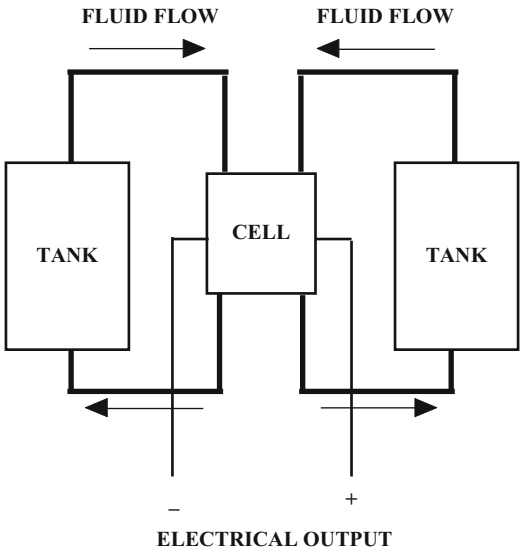

Fig. 22.35 General physical arrangement of a flow battery

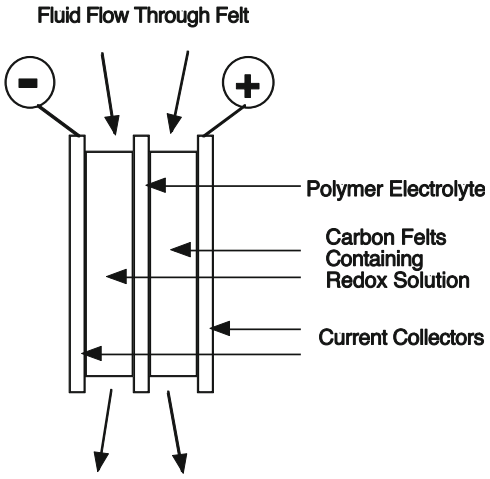

Fig. 22.36 The cell portion of the system. In some cases there are multiple bipolar cell configurations

compartments. This means that the capacity is not fixed by the cell dimensions, but is determined by the size of the liquid electrode reactant tanks. This can result in very large capacities, and is one of the potential advantages of flow battery systems. Thus flow batteries deserve consideration for relatively large stationary applications, such as remote solar or wind installations, whose outputs are dependent upon the time of day and/or the weather.

Table 22.2 Various redox systems used in flow batteries

System	Negative electrode reactant	Positive electrode reactant	Nominal voltage
V/Br	V	Bromine	1.0
Cr/Fe	Cr	Fe	1.03
V/V	V	V	1.3
Sulfide/Br	Polysulfide	Bromine	1.54
Zn/Br_2	Elemental Zinc	Bromine	1.75
Ce/Zn	Zn	Ce	<2

The open circuit voltage across the electrolyte is determined by the difference in the chemical potentials on its two sides. As current passes through the cell protons are transferred, changing the pH, so that the ionic compositions of the two electrode reactant fluids gradually change. Thus the cell potential varies with the state of charge. The change in the voltage with the amount of charge passed depends, of course, upon the size of the tanks.

Some of the redox systems have been explored are listed in Table 22.2.

A general discussion of these various alternatives can be found in reference [58].

There is some confusion in the terminology used to describe these systems, for the liquid reactants on the two sides are sometimes called "electrolytes," even though they do not function as electrolytes in the battery sense. Additionally, the liquid reactant on the negative side of the cell is sometimes called the "anolyte," and that on the positive side of the cell the "catholyte."

One of the most attractive flow systems involves the vanadium redox system [59–65]. In this case the negative electrode reactant solution contains a mixture of V^{2+} and V^{3+} ions, whereas the positive electrode reactant solution contains a mixture of V^{4+} and V^{5+} ions. Charge neutrality requirements mean that when protons (H^+ ions) are added or deleted from such liquids by passage through the polymer electrolyte in the cell, the ratio of the charges on the redox species is varied. This changes the state of charge of the system.

These systems are generally assembled in the uncharged state, in which the chemical compositions of the two liquid reactants are the same. In the vanadium system, this is done by adding vanadyl sulfate to 2 M H_2SO_4, which gives an equal mixture of V^{3+} and V^{4+} ions. The system is then charged by passing current, causing the transport of protons through the polymer electrolyte, so that the ion contents on the two sides become different.

22.11.2 Redox Reactions in the Vanadium/Vanadium System

One can write the reactions in the electrode solutions of the vanadium system as

$$VO_2^+ + 2H^+ + e^- = VO^{2+} + H_2O \tag{22.2}$$

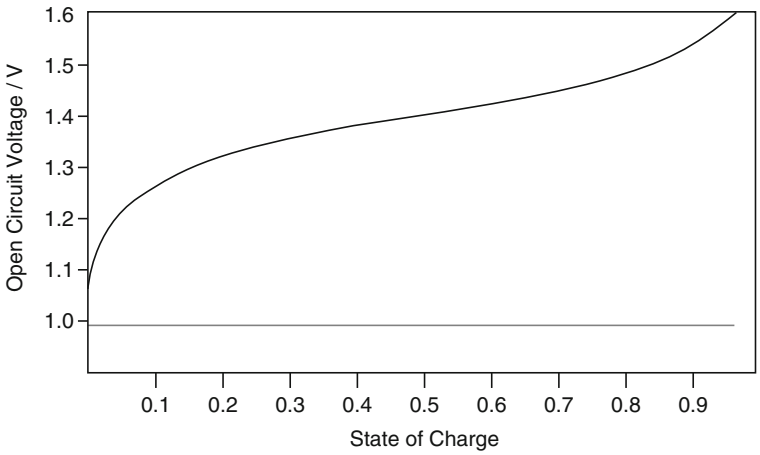

Fig. 22.37 Variation of the open circuit potential versus state of charge for the case of **a** V/V flow cell at 298 K

or, in terms of the vanadium ions:

$$V^{5+} + e^- = V^{4+} \tag{22.3}$$

in the positive electrode reactant solution, and

$$V^{2+} = V^{3+} + e^- \tag{22.4}$$

in the negative electrode reactant solution.

So that the overall reaction is

$$VO_2^{'} + 2H^+ + V^{2+} = VO^{2+} + H_2O + V^{3+} \tag{22.5}$$

or

$$V^{5+} + V^{2+} = V^{4+} + V^{3+} \tag{22.6}$$

The variation of the open circuit cell potential with the state of charge in the case of the V/V system with concentrations of 2 mol/liter of each V species is shown in Fig. 22.37. Typical operation would involve cycling between 20 and 80 % of capacity, and thus at voltages between 1.3 and 1.58 V.

Since each cell produces a relatively low voltage, such batteries generally contain a number of cells arranged in series in order to produce a greater overall output voltage. Parallel configurations can be used to provide higher currents. Depending upon the application, it may be desirable to permit relatively rapid charging, which may not be necessary during discharge. Thus it may be advantageous to include a mechanism to change the number of cells and their series/parallel arrangements during different operating conditions.

If all of the cells are fed from a common liquid supply, this can result in a large voltage applied across the liquid reactants and in the passage of a considerable amount of current. This is a form of self discharge, and is sometimes called shunt or bypass current. It is different, however, from the self discharge that results from neutral species, or neutral combinations of species, traveling through or around the electrolyte in other types of electrochemical systems.

Because there are no solid-state volume changes during charging and discharging, as are typical for electrochemical cells with solid electrodes, the components of the cells, as well as the total system, can have long lives. Thus long cycle life is generally not a problem, even with repeated deep charges and discharges.

The vanadium redox system can be used over a temperature range from 10 to 35 °C, and typically operates at or near ambient temperature. The solubility of (VO)SO_4 limits the energy capacity at lower temperatures. At higher temperatures the current density increases, but the cell voltage is reduced somewhat. The overall result is that the available power is greater at somewhat elevated temperatures. But care must be taken to not let the temperature go over 40 °C to avoid the precipitation of V_2O_5.

The electrode kinetics are good, and additional catalysts are not required. The coulometric and voltage efficiencies are high, except for the self-discharge mechanism mentioned above.

The specific energy and energy density are determined primarily by the electrode reactants themselves, which are the major components in these systems. Typical values are 15 Wh/kg and 18 Wh/l, and round trip efficiencies are typically 70–75 %.

Since the electrode reactants both consist of vanadium sulfate solutions in aqueous sulfuric acid, only differing by the oxidation states of the vanadium ions, contamination by leakage across the electrochemical cell membranes only results in some capacity loss, and is fully reversible. In flow batteries in which the ions are different on the two sides this can become a significant, and irreversible, problem.

Because the cell voltage is a function of the state of charge, it is possible to determine the state of charge of such systems remotely, which may be an advantage in some system installations. The cell design also makes monitoring of the voltage across each cell possible.

Since the cells can be configured in a variety of different series/parallel arrangements, the charging and discharging cycles can operate at different voltages. As a result, such a system can be used as a DC/DC converter.

The general attractive features of redox flow batteries include their long lifetime, which can involve an unlimited number of cycles of charging and deep discharge cycles. The typical reaction time of less than 100 milliseconds means that they can be used to support solar and wind systems that sometimes suffer large sudden transients in their output. The all-vanadium systems typically suffer only 1 % energy loss per year, and have a high level of safety, as they are nonflammable and nonexplosive. They require relatively little maintenance, and have the

advantage that the output and storage capacity are scalable independently of each other. Vanadium is environmentally friendly and recyclable.

The leading firm in this area is Cellstrom in Austria. As of the end of 2013 more than 50 CellCube systems had been sold to customers all over the world. This firm was founded in 2000 by DDr. Martha Schreiber, and was sold to the large German manufacturing firm Gildemeister in 2010. It is now named DMG MORI SEIKI.

22.11.3 Flow Batteries with a Modified Chemistry

A different approach to vanadium/vanadium flow batteries was introduced a few years ago by work at the Pacific Northwest National Laboratory led by Zhenguo (Gary) Yang. It involves the use of a sulfate/chloride mixed electrolyte, rather than the sulfate-only electrolyte [66, 67].

It was found that all four valence states of vanadium can be stable at concentrations up to 2.5 molar in a mixed solution containing 2.5 M SO_4^{2-} and 6 M Cl^- ions. This electrolyte produces a significantly higher energy capacity than in the standard sulfate-only electrolyte. Also, the operating temperature range can be increased from 10–40 °C to −5 to 50 °C by the use of the mixed acid electrolyte. The result is a significantly (about 70 %) increased energy density compared to the normal sulfate-only system. The voltage window of this mixed electrolyte is essentially the same as that of the standard 0.5 to 1.35 V, and there is no significant capacity fading upon cycling.

The attractive features of this new approach to flow batteries have led to the formation of the new firm UniEnergy Technologies, which intends to commercialize this technology.

22.12 All-Liquid Batteries

A relatively new concept that could be useful for large stationary storage applications is the use of an all-liquid three-component system that evolved from the PhD research of David Bradwell under the supervision of Prof. Donald Sadoway at MIT. The basic concept involves the use of two electronically-conducting liquid electrode materials that have densities different from that of an elevated temperature molten salt electrolyte, one lower, and the other greater. This leads to a three-layer configuration, with the electrolyte in the middle. The container, perhaps with a graphite insert, can act as the current collector for the lower electrode, and the upper electrode material can be contacted by an electronic conductor protruding from above. An inert gas cover, either nitrogen or argon, is needed to prevent reaction with air. This general configuration is illustrated schematically in Fig. 22.38.

Such a device can operate in the same way as conventional batteries with solid electrodes, with a charged species leaving one liquid electrode, travelling across the molten salt electrolyte, and reacting with the other liquid electrode material.

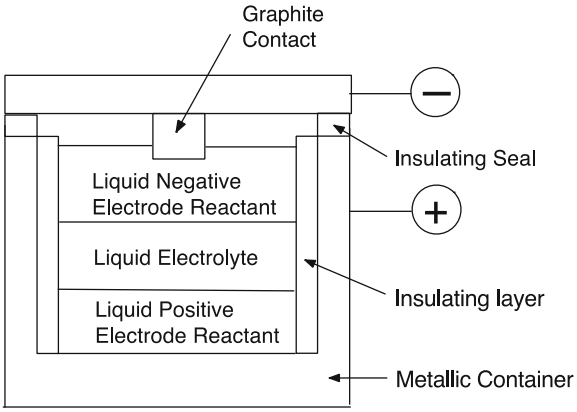

Fig. 22.38 Schematic Representation of an all-liquid cell

There are several potentially important advantages in such an all-liquid configuration, in which the components can be quite large, leading to high power. One is that there are no problems due to the dimensional changes in the electrode reactants, which can cause problems in common systems with fine solid particle battery electrodes. On the other hand, it is necessary to be aware of potential safety problems. Care must be taken to avoid contact of high temperature molten salts and highly reactive metals, such as magnesium, with air, for the results could be catastrophic.

Molten salt electrolytes can have conductivities much greater than both the sulfuric acid and KOH used in aqueous batteries, and the organic solvent electrolytes in lithium batteries. And with the possibility that all-liquid cells can be designed to have large area electrodes in contact with high conductivity electrolyte materials, it is reasonable to expect that such all-liquid cells can operate at very high power values.

An early example of this type of cell was the use of a heavy positive electrode material such as antimony, with a density of 6.5 g/cm^3, on the bottom, and magnesium, a relatively light negative electrode material with a density of 1.6 g/cm^3, on the top, with a mixed chloride electrolyte that has an intermediate density, 4.0 g/cm^3, in the middle [68]. This configuration can be written as a Mg/Sb cell. The reaction product was the solution of Mg into the liquid antimony. These cells were operated at 700 °C, and the open circuit voltage was only about 0.44 V.

Another design alternative can be used when both electrode materials are heavier than the electrolyte. An example of this type would be the use of Zn (density of 7.1 g/cm3) as negative electrode, Te (density 6.3 g/cm3) as positive electrode, and an electrolyte of $ZnCl_2$ (density 2.9 g/cm3). This is shown schematically in Fig. 22.39.

After the exploration of a number of other possible chemical systems, recent development efforts have focused on the use of molten lithium as the negative electrode, and an antimony–lead alloy, on the positive side of the cell [68, 69]. The advantage of the use of the antimony–lead alloy is that it can lead to a substantial reduction in the melting point relative to antimony itself, reducing the minimum operating temperature of such cells. This can be seen from the Pb-Sb phase diagram in Fig. 22.40.

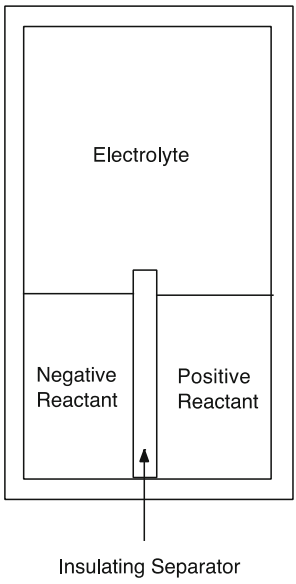

Fig. 22.39 Schematic view of a cell in which both electrode materials have greater densities than the liquid electrolyte

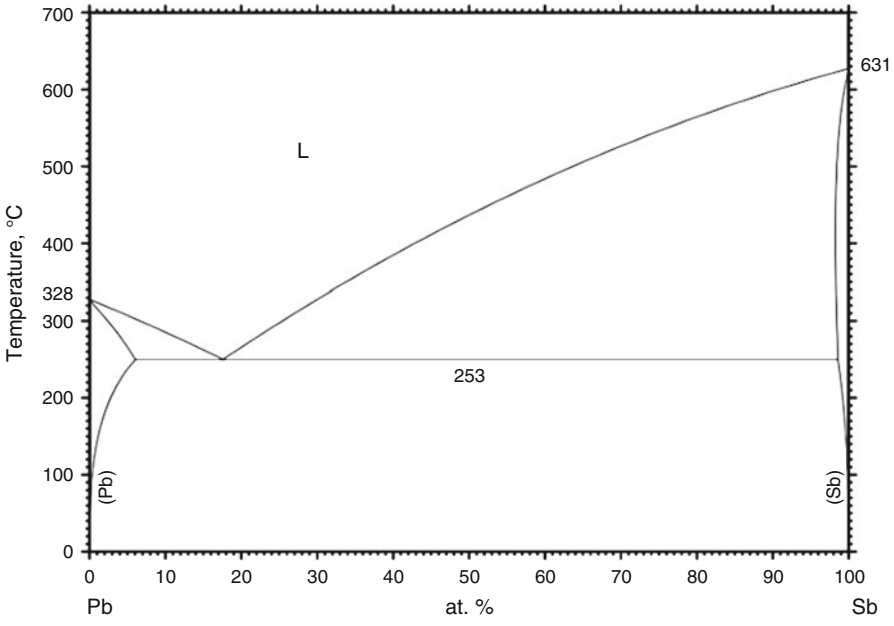

Fig. 22.40 Antimony–lead phase diagram

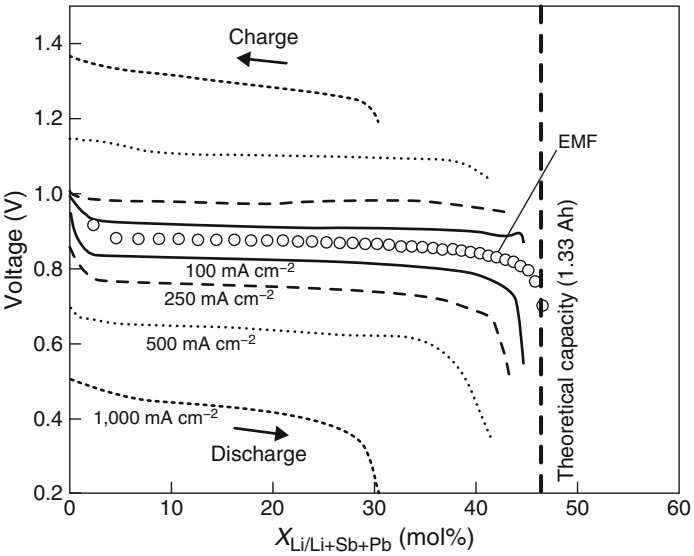

Fig. 22.41 Charge–Discharge Behavior of Li/Pb-Sb Battery at 450 °C. From ref. [69]

Cells with the Li/Pb-Sb chemistry operating at 450–500 °C have an open circuit voltage of about 0.9 V and operate between 0.75 and 0.65 V at a 5-h discharge rate. At discharge rates of C/2 the Coulombic efficiency is over 98 %.

Although this salt electrolyte is liquid in the charged state, two phases are present on discharge, so that care must be given to the discharge rate to avoid transient local freezing. While this may not be a significant problem for relatively short pulses, it would be expected to limit performance at higher rates over an extended period of time. That does not seem to be a problem, however, if the battery is charged until the electrolyte is fully liquid after each cycle. This is due to the fortuitous fact that the transient solid product is Li_3Sb, which has been known for a long time to have an unusually rapid rate of chemical diffusion.

The charge–discharge behavior over a range of current densities at 450 °C is shown in Fig. 22.41.

The cost of such systems will depend to a large extent upon the identity of the materials used in both the electrodes and the electrolyte, which are much less expensive than those used in many other current battery systems. Thus they should be quite low, perhaps between those of pumped hydro and compressed air systems.

References

1. Hunt T, Clark N, Baca W. 18th International Seminar on Double Layer Capacitors and Hybrid Energy Storage Devices, Fort Lauderdale, FL (2008)

2. Furukawa J (2013) Development of Ultra Battery. Furukawa Review No. 43, Furukawa Electric Co
3. Furukawa J, Takada T, Monma D, Lam LT (2010) J Power Sources 195:1241
4. Joo S-K, Raistrick ID, Huggins RA (1985) Mater Res Bull 20:897
5. Joo S-K, Raistrick ID, Huggins RA (1985) Mater Res Bull 20:1265
6. Joo S-K, Raistrick ID, Huggins RA (1985) Solid State Ion 17:313
7. Joo S-K, Raistrick ID, Huggins RA (1986) Solid State Ion 18/19:592
8. Inaguma Y et al (1993) Solid State Commun 86:689
9. Kawai H, Kuwano J (1994) J Electrochem Soc 141:L78
10. Inaguma Y, Chen L, Itho M, Nakamura T (1994) Solid State Ion 70/71, 196:203
11. Inaguma Y, Yu J, Shan Y-J, Itho M, Nakamura T (1995) J Electrochem Soc 142:L8
12. Robertson AD, Garcia Martin S, Coats A, West AR (1995) J Mater Chem 5:1405
13. Birke P, Scharner S, Huggins RA, Weppner W (1997) J Electrochem Soc 144:L167
14. Sauvage F, Laffont L, Tarascon J-M, Baudrin E (2007) Inorg Chem 46:3289
15. Doeff MM, Richardson TJ, Kepley L (1996) J Electrochem Soc 143:2507
16. Doeff MM, Anapolsky A, Edman L, Richardson TJ, DeJonghe LC (2001) J Electrochem Soc 148:A230
17. Whitacre JF, Tevar A, Sharma S (2010) Electrochem Commun 12:463
18. Tevar AD, Whitacre JF (2010) J Electrochem Soc 157:A870
19. Cao Y, Xiao L, Wang W, Choi D, Nie Z, Yu J, Saraf LV, Yang Z, Liu J (2011) Adv Mater 23:3155
20. Whitacre JF, Wiley T, Shanbhag S, Wenzhuo Y, Mohamed A, Chun SE, Weber E, Blackwood D, Lynch-Bell E, Gulakowski J, Smith C, Humphreys D (2012) J Power Sources 213:255
21. Zhou X, Guduru RK, Mohanty P (2013) J Mater Chem A 1:2757
22. Huggins RA (1997) Ionics 3:379
23. Huggins RA (1998) Solid State Ion 113:533
24. Robin MB, Day P (1967) Adv Inorg Chem Radiochem 10:247
25. Brown J (1724) Philos Trans 33:17
26. Weiser HB (1938) Inorganic Colloid Chemistry, Vol 3, Colloidal Salts. John Wiley & Sons, New York, p 343
27. Keggin JF, Miles FD (1936) Nature 577
28. Wilde RE, Ghosh SN, Marshall BJ (1970) Inorg Chem 9:2512
29. Siperko LM, Kuwana T (1983) J Electrochem Soc 130:396
30. Crumblis AL, Lugg PS, Morosoff N (1984) Inorg Chem 23:4701
31. Armand MB, Whittingham MS, Huggins RA (1972) Mater Res Bull 7:101
32. Oi T (1986) In Annual Review of Materials Science R. A. Huggins (Eds), 16, p. 185
33. Itaya K, Uchida I, Neff VD (1986) Acc Chem Res 19:162
34. Itaya K, Ataka T, Toshima S (1982) J Am Chem Soc 104:4767
35. Neff VD (1985) J Electrochem Soc 132:1382
36. Honda K, Hayashi H (1987) J Electrochem Soc 134:1330
37. Wessells CD. PhD Dissertation, Stanford University (2012)
38. Wessells CD, Huggins RA, Cui Y (2011) Nat Commun 2:550
39. Wessells CD, Peddada SV, Huggins RA, Cui Y (2011) Nano Lett 11:5421
40. Wessells CD, Peddada SV, McDowell MT, Huggins RA, Cui Y (2012) J Electrochem Soc 159:A98
41. Wessells CD, McDowell MT, Peddada SV, Pasta M, Huggins RA, Cui Y (2012) ACS Nano 6:1688
42. Wang RY, Wessells CD, Huggins RA, Cui Y (2013) Nano Lett 13:5748
43. Lee H-W, Pasta M, Wang RY, Ruffo R, Cui Y (2014) Faraday Disc 176:69
44. Lee H-W, Wang RY, Pasta M, Lee SW, Liu N, Cui Y (2014) Nat Commun 5:5280
45. Eftekhari A (2004) J Power Sources 126:221
46. Lu Y, Wang L, Cheng J, Goodenough JB (2012) Chem Commun 48:6544

47. Wang L, Lu Y, Liu J, Xu M, Cheng J, Zhang D, Goodenough JB (2013) Angew Chem Int Ed 52:1964
48. Pasta M, Wessells CD, Huggins RA, Cui Y (2012) Nat Commun 3:2139
49. Huggins RA (2013) J Electrochem Soc 160:A3020
50. Pasta M, Wessells CD, Liu N, Nelson J, McDowell MT, Huggins RA, Toney MF, Cui Y (2014) Nat Commun 5:3007
51. Wessells C, Ruffo R, Huggins RA, Cui Y (2010) Electrochem Solid-State Lett 13:A59
52. Wessells C, Huggins RA, Cui Y (2011) J Power Sources 196:2884
53. Radzilowski RH, Yao YF, Kummer JT (1969) J Appl Phys 40:4716
54. Whittingham MS, Huggins RA (1971) J Chem Phys 54:414
55. Weber N, Kummer JT (1967) Proc Ann Power Sources Conf 21:37
56. Yao YFY, Kummer JT (1967) J Inorg Nucl Chem 29:2453
57. Sudworth JL, Tilley AR (1985) The Sodium Sulphur Battery. Chapman and Hall, London
58. Gahn RF, Hagedorn NH, Ling JS. DOE/NASA/12726-21 (1983)
59. Ponce de Leon C, Frias-Ferrer A, Gonzales-Garcia J, Szanto DA, Walsh FC (2006) J Power Sources 160:716
60. Sum E, Skyllas-Kazacos M (1985) J Power Sources 15:179
61. Sum E, Rychcik M, Skyllas-Kazacos M (1985) J Power Sources 16:85
62. Skyllas-Kazacos M, Rychcik M, Robins R, Fane A, Green M (1985) J Electrochem Soc 133:1057
63. Rychcik M, Skyllas-Kazacos M (1987) J Power Sources 19:45
64. Rychcik M, Skyllas-Kazacos M (1988) J Power Sources 22:59
65. Skyllas-Kazacos M, Grossmith F (1987) J Electrochem Soc 134:2950
66. Li L, Kim S, Wang W, Vijayakumar M, Nie Z, Chen B, Zhang J, Xia G, Hu J, Graff G, Liu J, Yang Z (2011) Adv Energy Mater 1:394
67. Wang W, Luo Q, Li B, Wei X, Li L, Yang Z (2013) Adv Funct Mater 23:970
68. Bradwell DJ, Kim H, Sirk AHC, Sadoway DR (2012) J Am Chem Soc 134:1895
69. Kim H, Boysen DA, Newhouse JM, Spatocco BL, Chung B, Burke PJ, Bradwell DJ, Jiang K, Tomaszowska AA, Wang K, Wei W, Ortiz LA, Barriga SA, Poizeau SM, Sadoway DR (2013) Chem Rev 113:2075
70. Wang K, Jiang K, Chung B, Ouchi T, Burke PJ, Boysen DA, Bradwell DJ, Kim H, Muecke U, Sadoway DR (2014) Nature 514:348